Results in Chemistry 6 (2023) 101158

Contents lists available at ScienceDirect

Results in Chemistry

journal homepage: www.sciencedirect.com/journal/results-in-chemistry

Purification of metronidazole and penicillin-G contaminated water by MOF-5 imprinted cobalt ferrite

Babatunde K. Adeleke [a], Olamide A. Olalekan [a], Adewale Adewuyi [a,*], Woei Jye Lau [b], Olalere G. Adeyemi [a]

[a] Department of Chemical Sciences, Faculty of Natural Sciences, Redeemer's University, Ede, Osun State, Nigeria
[b] Faculty of Chemical and Energy Engineering, Universiti Teknologi Malaysia, 81310 Skudai, Johor, Malaysia

ARTICLE INFO

Keywords:
Adsorption
Antibiotics
Metal organic framework

ABSTRACT

Water contamination by antibiotics such as metronidazole (MTZ) and penicillin-G (PCG) is a serious concern. Therefore, this study evaluates the potential of cobalt ferrite ($CoFe_2O_4$) and cobalt ferrite imprinted terephthalic acid-zinc metal–organic framework ($CoFe_2O_4$@MOF-5) as adsorbents for the removal of MTZ and PCG from contaminated water sources. The scanning electron micrograph revealed the surfaces of $CoFe_2O_4$ and $CoFe_2O_4$@MOF-5 to be heterogeneous with irregularly shaped particles, while the Brunauer-Emmett-Teller (BET) surface area was found to be 16.63 and 12.41 m^2/g for $CoFe_2O_4$ and $CoFe_2O_4$@MOF-5, respectively. The X-ray diffraction (XRD) revealed a crystallite size of 28.31 nm for $CoFe_2O_4$ and 29.01 nm for $CoFe_2O_4$@MOF-5. $CoFe_2O_4$@MOF-5 exhibited higher sorption capacity towards MTZ (94.47 mg g^{-1}) and PCG (90.28 mg g^{-1}) than values displayed by $CoFe_2O_4$ towards MTZ (50.41 mg g^{-1}) and PCG (55.76 mg g^{-1}). The sorption process may be described by the Langmuir and Freundlich isotherms with a quantum chemical simulation analysis that revealed the process mechanism to be via electronic interaction. The regeneration capacity of $CoFe_2O_4$@MOF-5 was higher than that of $CoFe_2O_4$, with a regeneration capacity of 91.71 % for MTZ and 89.31 % for PCG at the 10th regeneration cycle. Furthermore, $CoFe_2O_4$@MOF-5 compared favourably with previously reported adsorbents. The study's findings revealed $CoFe_2O_4$@MOF-5 as a promising material for the purification of water contaminated with MTZ and PCG.

Introduction

Pollution of drinking water sources, such as surface and underground water systems, by antibiotics, is a concern that requires immediate attention. The consequence of the concern is far-reaching and may have a devastating effect. When antibiotics are present in drinking water sources, they may break down into simple or complex molecules that may be toxic to humans and the environment [1]. Apart from this, studies have shown the emergence of drug-resistant strains of pathogenic organisms due to the persistence of antibiotics in environmental water systems [2]. Antibiotics have been reported in surface water, industrial effluents, hospital wastes and bottled water [3–7]. Developing a method for efficiently removing antibiotics from water and protecting safe drinking water is essential. Several antibiotics have been reported in the water system; however, metronidazole (MTZ) and penicillin-G (PCG) are common antibiotics reported in drinking water sources [8–10]. Therefore, this study focuses on MTZ and PCG because they are commonly found in environmental water systems and frequently reported in drinking water sources.

MTZ belongs to the nitroimidazole class of antibiotics [11,12], while PCG belongs to the beta-lactam group of antibiotics [13]. MTZ and PCG are used to treat many infections and diseases. Although they are prescription drugs, they may be purchased over the counter in many developing countries due to poor enactment of government regulations. Overdoses of MTZ and PCG are excreted by human body systems, which remains one of the points of MTZ and PCG getting into the environment. Inadequate disposal of expired MTZ and PCG or their containers has contributed to their environmental presence. A few studies have reported the presence of MTZ and PCG as contaminants in water systems [9,10,14–16]. It is crucial that they are removed from the water before they are metamorphosed into a chemical threat in drinking water. Several methods are known for water treatment, including physical and chemical treatment. Most methods have shortcomings, such as being expensive, forming toxic side products and having poor removal

* Corresponding author.
E-mail address: walexy62@yahoo.com (A. Adewuyi).

https://doi.org/10.1016/j.rechem.2023.101158
Received 14 September 2023; Accepted 7 October 2023
Available online 10 October 2023

mechanisms. Adsorption remains an effective method for water purification which can be used on a large-scale process.

Adsorption has shown a capacity to remove organic molecules in water [17–21] with unique properties such as a high removal rate, selectivity, and stability. One significant advantage of adsorption is the recovery of pollutants from the solution without decomposition. The fact that contaminants can be recovered in their original form shows that they can be reused. Some adsorbents have been reported for removing antibiotics in water [22–25]. However, some of these adsorbents are expensive to prepare or use to remove pollutants in water. Some of them need better regeneration for reuse which is a disadvantage. Therefore, this work proposes the use of nanomaterial for the removal of MTZ and PCG in water. Ferrites are examples of nanomaterials that can be used to achieve this purpose.

Ferrites are materials of the general formula MFe_2O_4. Their unique properties, such as surface area, magnetism, permeability, electrical conductivity and thermal stability, may be attributed to their small size. They have been used as adsorbents for removing organic pollutants in water systems [26–29]. Butylated hydroxyanisole and butylated hydroxytoluene were adsorbed in water by $CuFe_2O_4$ [30]. Similarly, $SrFe_2O_4$ expressed an enhanced adsorptive capacity towards methyl orange, phenolphthalein and bromothymol blue in an aqueous solution [31].

Despite the success achieved with ferrite, they may agglomerate, reducing their surface area and adsorbent capacity [32]. In this study, cobalt ferrite ($CoFe_2O_4$) was proposed as an adsorbent for removing MTZ and PCG from water. Furthermore, to improve the stability of $CoFe_2O_4$, it was incorporated with a metal–organic framework, terephthalic acid-zinc complex (MOF-5), which is a three-dimensional structure with high stability [33] and can be used for water treatment [34]. Incorporation of $CoFe_2O_4$ in MOF-5 to produce $CoFe_2O_4$@MOF-5 may serve as means to reducing agglomeration and improving performance of adsorbent. A previous study revealed the capacity of $CuCoFe_2O_4$@chitosan to remove tetracycline in water but with an efficiency of less than 100 % [35]. Performance for removing antibiotics was enhanced when $NiFe_2O_4$ was incorporated in a bimetallic MOF for removing ciprofloxacin and tetracycline in water [36]. Therefore, the present study aimed at producing $CoFe_2O_4$ and $CoFe_2O_4$@MOF-5 via a simple reaction route to remove MTZ and PCG from aqueous systems.

Materials and methods

Materials

Sodium hydroxide (NaOH), zinc acetate dihydrate ($(CH_3COO)_2Zn{\cdot}2H_2O$), hydrochloric acid (HCl), cobalt chloride hexahydrate ($CoCl_2{\cdot}6H_2O$), terephthalic acid, oleic acid, MTZ, triethylamine, PCG, ethanol, ferric chloride hexahydrate ($FeCl_3{\cdot}6H_2O$) and other chemicals used in the study were bought from Aldrich Chemical Co., England. They are of ACS reagent grade.

Synthesis of $CoFe_2O_4$ particles

$CoFe_2O_4$ particles were prepared via coprecipitation by mixing solutions of $FeCl_3{\cdot}6H_2O$ (0.4 M) and $CoCl_2{\cdot}2H_2O$ (0.2 M) in a 1-L beaker at 303 K for 1 h in the presence of oleic acid (10 mL) as capping agent. The temperature was gradually raised to 343 K while stirring continuously for 1 h. Black precipitates were formed on the dropwise addition of NaOH solution (2 M), keeping the pH (at 10–12) while stirring at 343 K. The temperature of the reaction mixture was cooled to 303 K and filtered. The precipitates obtained were washed with ethanol and deionized water until neutral to litmus. The precipitates were oven-dried at 105 °C for 3 h and kept in the furnace at 823.15 K for 18 h.

Synthesis of MOF-5

MOF-5 was prepared by mixing terephthalic acid (4.10 mmol), triethylamine (28.00 mL) and $(CH_3COO)_2Zn{\cdot}2H_2O$ (7.24 mmol) together in a 500-mL round bottom flask at room temperature (303 K) for 24 h. The white product formed was filtered and washed with deionized water until neutral to litmus. The product was oven-dried at 343 K for 2 h to obtain a white powder.

Synthesis of $CoFe_2O_4$@MOF-5

Solution of MOF-5 was prepared by dissolving MOF-5 (2.50 g) in triethylamine (50.00 mL) in a round bottom flask and refluxed at 343 K for 1 h. $CoFe_2O_4$ particles (2.50 g) were added to the solution of MOF-5 under reflux while the stirring was maintained for 2 h. The product formed was filtered, washed severally with deionized water until neutral to litmus and oven-dried at 343 K for 8 h.

Characterisation of $CoFe_2O_4$ and $CoFe_2O_4$@MOF-5

The Fourier transformed infrared (FTIR) spectroscopy analysis of $CoFe_2O_4$ and $CoFe_2O_4$@MOF-5 was recorded on Perkin Elmer from 400 to 4000 cm^{-1} while the thermogravimetric (TGA) analysis was achieved on TGA Q500 V20 (TA Instruments). The surface morphology of $CoFe_2O_4$ and $CoFe_2O_4$@MOF-5 was evaluated on scanning electron microscopy (SEM, TM 3000–123109-05) and energy-dispersive X-ray spectroscopy (EDX). Brunauer-Emmett-Teller (BET) surface area of $CoFe_2O_4$ and $CoFe_2O_4$@MOF-5 were determined via the nitrogen gas adsorption process (Micromeritics, TriStar II 3020 version 3.02). The XRD patterns of $CoFe_2O_4$ and $CoFe_2O_4$@MOF-5 were recorded at 2θ on a diffractometer (Panalytical Empyrean, Cu radiation), measured at a range 5.00–90.00°.

Batch adsorption study

The batch adsorption of MTZ or PCG by $CoFe_2O_4$ and $CoFe_2O_4$@MOF-5 was conducted by contacting 0.10 g of $CoFe_2O_4$ or $CoFe_2O_4$@MOF-5 with solution (100 mL) of MTZ or PCG with concentration ranging from 5.00 to 100.00 mg L^{-1} at an initial pH of 7.0 in a conical flask (250 mL) while shaking at 150 rpm at room temperature (303 K) for 120 min. Clear samples of MTZ or PCG were withdrawn at an interval from the test solution and analyzed using a UV–visible spectrophotometer (Spectroquant Pharo 300) to determine the concentration of MTZ or PCG making use of a pre-determined calibration curve for MTZ and PCG. The actual values of MTZ (λ_{max} = 320 nm) and PCG (λ_{max} = 283 nm) were read at their respective maximum absorbance wavelength. The effect of adsorbent weight on the process performance was evaluated by varying the weight of $CoFe_2O_4$ or $CoFe_2O_4$@MOF-5 from 0.1 to 0.5 g at pH 7 and a concentration of 100 mg L^{-1} for 120 min. The effect of solution pH on the process performance was checked at a concentration of 100.00 mg L^{-1} and 0.1 g of $CoFe_2O_4$ or $CoFe_2O_4$@MOF-5 while varying pH from 1 to 13. The process temperature was varied from 303 to 323 K to understand the effect of temperature on the sorption process of MTZ or PCG by $CoFe_2O_4$ (0.1 g) or $CoFe_2O_4$@MOF-5 (0.1 g) at a concentration of 100.00 mg L^{-1} for 120 min.

The performance of $CoFe_2O_4$ or $CoFe_2O_4$@MOF-5 was estimated by determining their adsorption capacity (mg g^{-1}) at equilibrium (q_e) and time t (q_t) and percentage removal (%) for the removal of MTZ and PCG from aqueous solution as shown in Eq. 1(a-d).

$$q_t = \frac{(C_o - C_t)V}{m} \tag{1a}$$

$$q_e = \frac{(C_o - C_e)V}{m} \tag{1b}$$

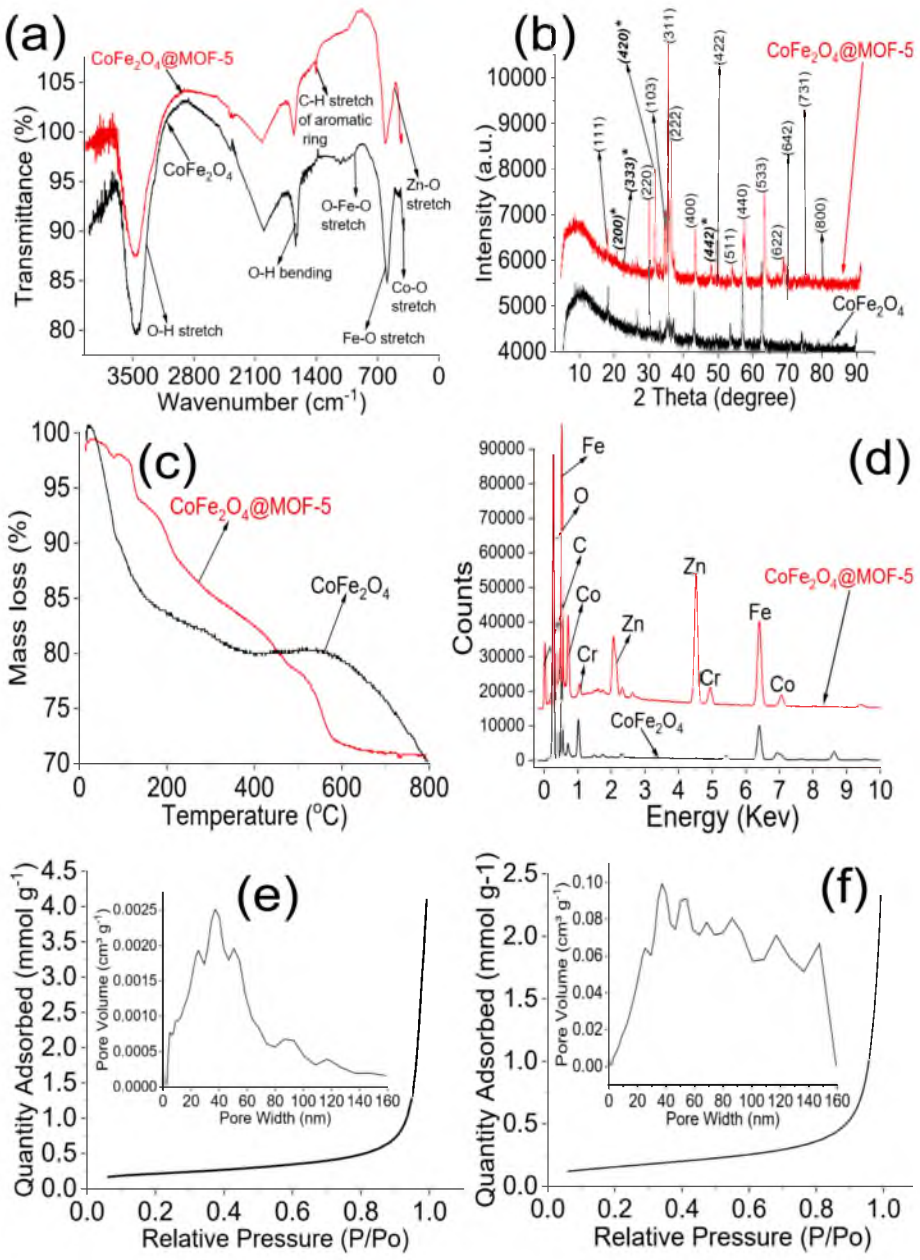

Fig. 1. (a) FTIR spectra of $CoFe_2O_4$ and $CoFe_2O_4$@MOF-5, (b) XRD pattern of $CoFe_2O_4$ and $CoFe_2O_4$@MOF-5, (c) TGA analysis of $CoFe_2O_4$ and $CoFe_2O_4$@MOF-5, (d) EDS results of $CoFe_2O_4$ and $CoFe_2O_4$@MOF-5, (e) BET of $CoFe_2O_4$ and (f) BET of $CoFe_2O_4$@MOF-5.

$$Removal = \frac{(C_o - Ct)}{Co} x100 \quad (1c)$$

$$q_t = \frac{(\%removal \mathrm{x} C_o \mathrm{x} V)}{100 \mathrm{x} m} \quad (1d)$$

The initial, final and equilibrium concentrations (mg L^{-1}) of MTZ and PCG are represented as C_o, C_t and C_e, respectively. The weight (in grams) of $CoFe_2O_4$ or $CoFe_2O_4$@MOF-5 and volume (in litre) of the test solution ($CoFe_2O_4$ or $CoFe_2O_4$@MOF-5) are represented as m and V, respectively.

Desorption and regeneration studies

The solvent regeneration method was employed to remove MTZ and PCG from the surface of $CoFe_2O_4$ and $CoFe_2O_4$@MOF-5. The solvent used for the desorption were selected based on the safety level of solvent as well as the solubility of MTZ and PCG. Firstly, 0.5 g of $CoFe_2O_4$ or $CoFe_2O_4$@MOF-5 was contacted with the test solutions (100 mL) of MTZ (100.00 mg L^{-1}) or PCG (100.00 mg L^{-1}) in an Erlenmeyer flask for 120 min at 150 rpm and 303 K. It was filtered on 0.22-μm Whatman membrane filter and the residue ($CoFe_2O_4$-MTZ/PCG or $CoFe_2O_4$@MOF-5-MTZ/PCG) obtained was air dried overnight. Finally, the adsorbed MTZ or PCG was desorbed from the dried residue ($CoFe_2O_4$-MTZ/PCG or $CoFe_2O_4$@MOF-5-MTZ/PCG) by shaking the residue at 150 rpm in the selected solvents, which are deionized water, methanol, HCl (0.1 M), NaOH (0.1 M) or a mixture of methanol:HCl (0.1 M) at ratio (2:1) for 120 min in an Erlenmeyer flask at room temperature. Clear samples of MTZ and PCG were withdrawn to determine the concentration UV–visible spectrophotometer (Spectroquant Pharo 300). The desorption (%) of MTZ or PCG from the surfaces of $CoFe_2O_4$ or $CoFe_2O_4$@MOF-5 was calculated from the amount of MTZ and PCG desorbed (q_d) from $CoFe_2O_4$ or $CoFe_2O_4$@MOF-5 at equilibrium and amount of MTZ and PCG adsorbed by $CoFe_2O_4$ or $CoFe_2O_4$@MOF-5 at equilibrium as shown in Eq. (2);

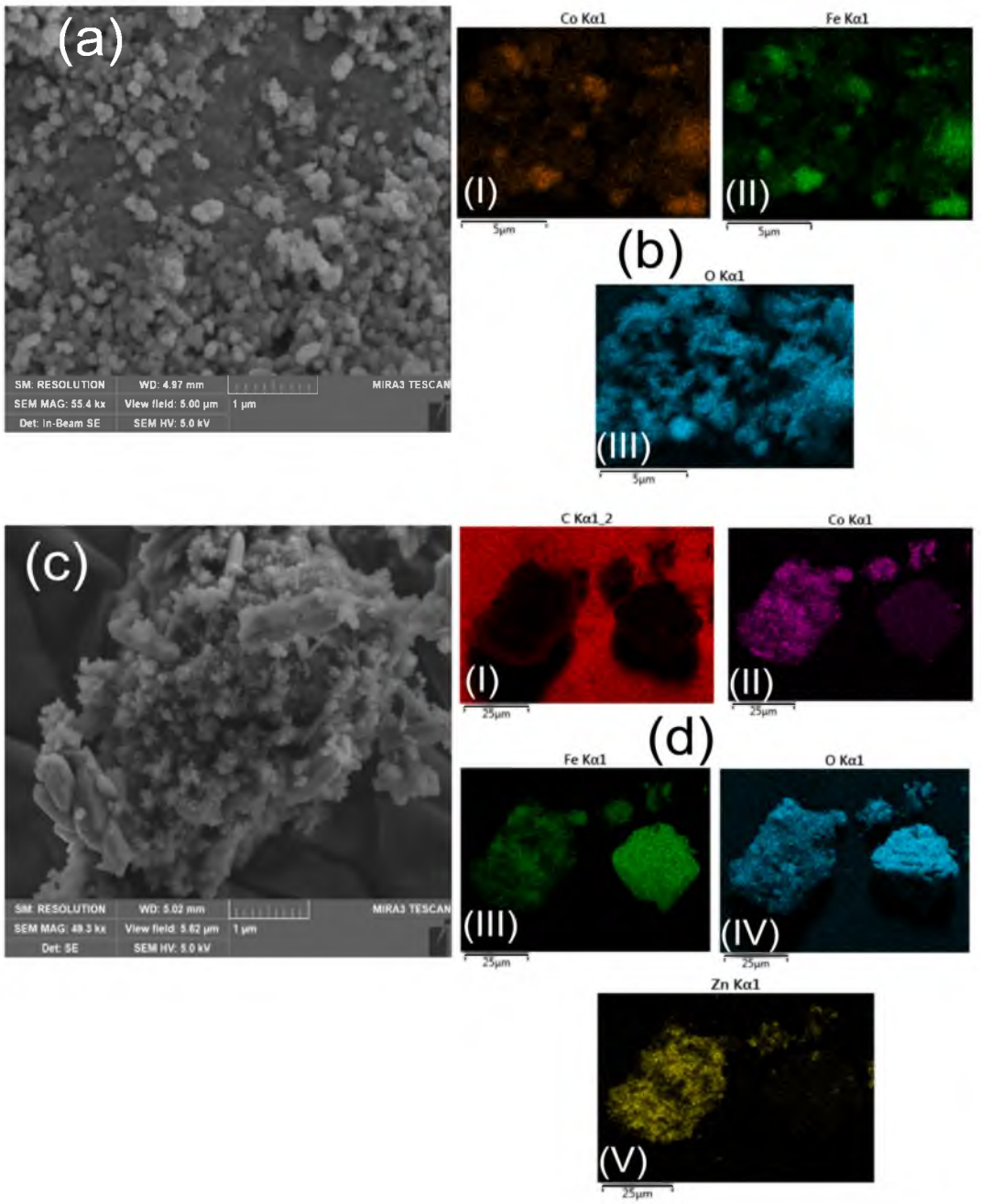

Fig. 2. (a) SEM image of $CoFe_2O_4$ and its elemental surface mapping (b I-III), (c) SEM image of $CoFe_2O_4$@MOF-5 and its elemental surface mapping (d I-V).

$$Desorption = \frac{q_d(desorption)}{q_a(adsorption)} \text{x}100 \quad (2)$$

Methanol gave the best result among the solvents used for the desorption study. Therefore, the regeneration study for $CoFe_2O_4$ and $CoFe_2O_4$@MOF-5 was carried out using methanol. The adsorption–desorption process was performed repeatedly for 10 consecutive cycles to investigate the stability of $CoFe_2O_4$ and $CoFe_2O_4$@MOF-5.

Quantum chemical simulation

The mechanism for removing MTZ and PCG by $CoFe_2O_4$ and $CoFe_2O_4$@MOF-5 was described by quantum chemical analysis using Density Functional Theory (DFT) electronic structure programs (B3LYP/6-31G level theory on Spartan 14.1 software). Quantum chemical parameters for MTZ and PCG were determined by modelling their molecular electronic structures, including the distribution of the frontier molecular orbitals, highest occupied molecular orbital (HOMO) of $CoFe_2O_4$ and $CoFe_2O_4$@MOF-5 and lowest unoccupied molecular orbital (LUMO) of $CoFe_2O_4$ and $CoFe_2O_4$@MOF-5. The processes' energy gaps (ΔE) were calculated from Eq. (3).

$$\Delta E = E_{LUMO} - E_{HOMO} \quad (3)$$

Similarly, the absolute hardness (η) was determined based on Eq. (4).

$$\eta = \frac{E_{LUMO} - E_{HOMO}}{2} \quad (4)$$

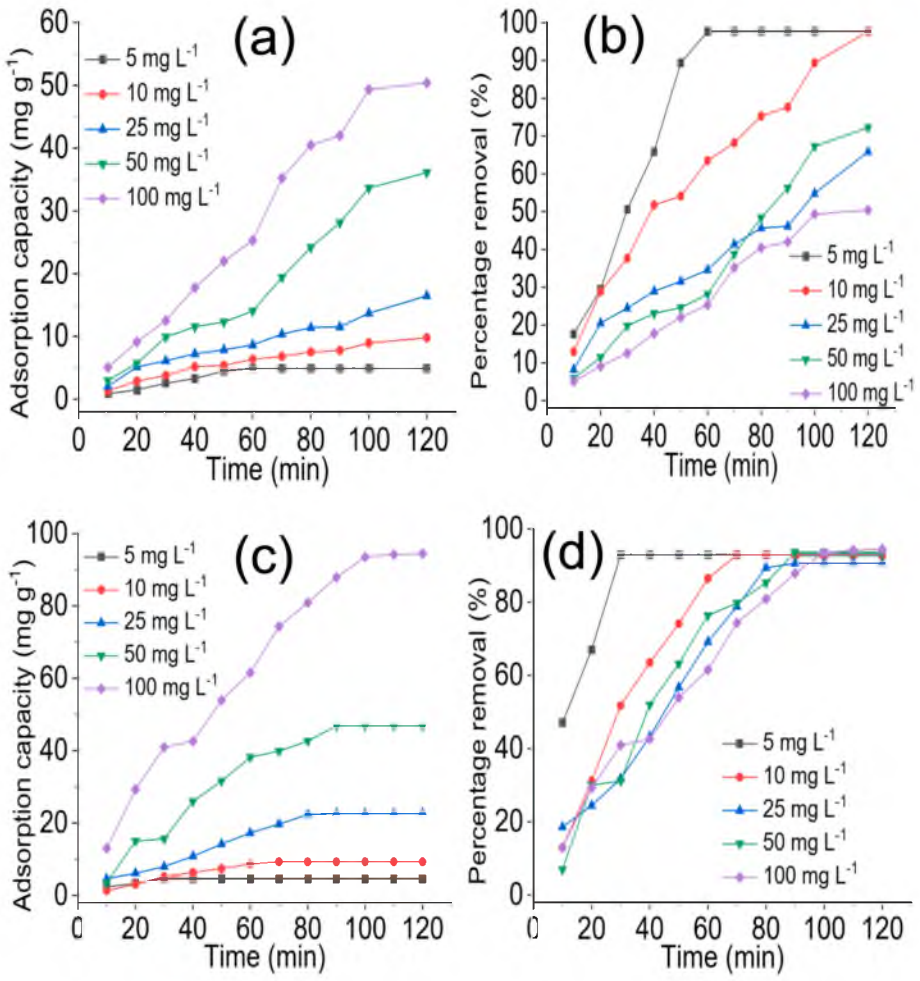

Fig. 3. (a) Time dependent adsorption capacity expressed by $CoFe_2O_4$ towards MTZ at solution concentration of 100 mg L^{-1}, speed of 150 rpm and pH of 7, (b) time dependent percentage removal expressed by $CoFe_2O_4$ towards MTZ at solution concentration of 100 mg L^{-1}, speed of 150 rpm and pH of 7, (c) time dependent adsorption capacity expressed by $CoFe_2O_4$@MOF-5 towards MTZ at solution concentration of 100 mg L^{-1}, speed of 150 rpm and pH of 7 and (d) time dependent percentage removal expressed by $CoFe_2O_4$@MOF-5 towards MTZ at solution concentration of 100 mg L^{-1}, speed of 150 rpm and pH of 7.

Results and discussion

Synthesis and characterization of $CoFe_2O_4$ and $CoFe_2O_4$@MOF-5

The FTIR spectra for $CoFe_2O_4$ and $CoFe_2O_4$@MOF-5 shown in Fig. 1a revealed the vibrational frequencies of different functional groups present in them. A peak appeared at 3463 cm^{-1} in $CoFe_2O_4$ and $CoFe_2O_4$@MOF-5 was attributed to the OH stretching of the adsorbed water molecules on their surfaces. Subsequently, the peak at 1625 cm^{-1} was assigned to the OH bending frequencies of water molecules attached to the Fe ions [37,38]. The signal for the O-Fe-O vibration was found at 1018 cm^{-1}, while the Fe-O peak was detected at 672 cm^{-1}. The aromatic ring stretching, which appeared at 1408 cm^{-1} was only detected in the $CoFe_2O_4$@MOF-5 while it was missing in the $CoFe_2O_4$. The vibrational frequencies corresponding to Co-O and Zn-O are 410 and 402 cm^{-1}, respectively.

The diffraction pattern for $CoFe_2O_4$ and $CoFe_2O_4$@MOF-5 (Fig. 1b) revealed spinel structures with the most intense peak at $2\theta = 35.49°$ ($CoFe_2O_4$) and $2\theta = 35.51°$ ($CoFe_2O_4$@MOF-5) with planes corresponding to (103), (111), (200), (220), (222), (311), (333), (400), (420), (422), (440), (442), (511), (533), (622), (642), (731) and (800). However, peaks at (200), (333), (420) and (442) were only seen in $CoFe_2O_4$@MOF-5. These peaks are starred to distinguish them from peaks that appeared in $CoFe_2O_4$. The starred peaks in $CoFe_2O_4$@MOF-5 confirm the presence of MOF-5 structure in $CoFe_2O_4$@MOF-5 as previously reported [39–41]. The diffraction patterns correspond well with the structure of JCPDS No. 04–016-3954 for $CoFe_2O_4$ and JCPDS No. 96–432-6738 for MOF-5.

Furthermore, their average crystallite sizes (D) were determined from their reflections of (311) by the Debye-Scherrer's formula having K as a constant (0.89) and the X-ray wavelength as λ (1.5406 Å). To input the data for the calculation, the width of the diffraction line (β) and Bragg's angle (θ) were determined using Eq. (5) [42]:

$$D = \frac{K\lambda}{\beta Cos\theta} \tag{5}$$

The crystallite size of $CoFe_2O_4$ is estimated to be ~ 28.31 nm, while that of $CoFe_2O_4$@MOF-5 is 29.01 nm. The larger crystallite size of $CoFe_2O_4$@MOF-5 may be associated with the inclusion of MOF-5 in its structure. To better describe the effect of crystallite size, the relationship between the average diffusion time (τ) to the surfaces of $CoFe_2O_4$ and $CoFe_2O_4$@MOF-5 and the diffusion coefficient (F) may be examined by considering Eq. 6 [43,44]:

$$\tau = r^2\pi^2 F \tag{6}$$

The expression can be inferred to mean that when the value of F is large, the average diffusion time also becomes large. The larger the value of F, the longer it takes for adsorbate to get to the active sites on the adsorbents ($CoFe_2O_4$ and $CoFe_2O_4$@MOF-5). Therefore, the crystallite size is expected to be small for effective mass transfer of MTZ and

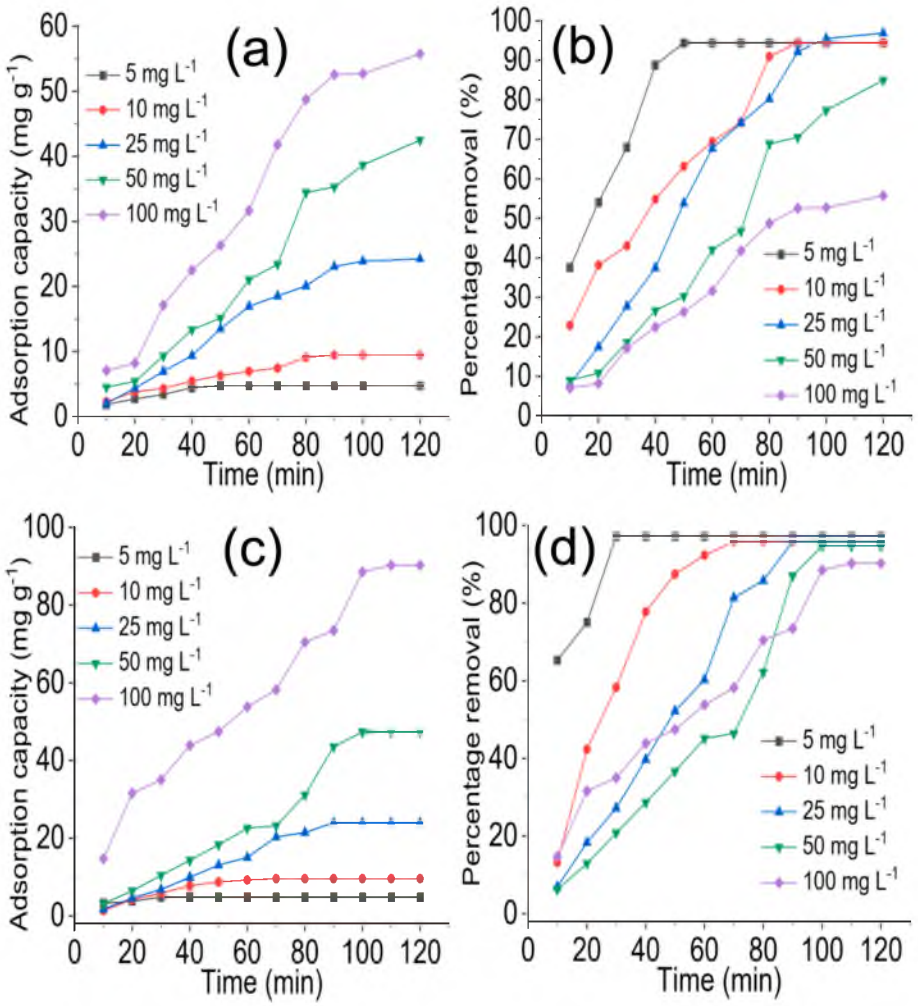

Fig. 4. (a) Time dependent adsorption capacity expressed by $CoFe_2O_4$ towards PCG at solution concentration of 100 mg L^{-1}, speed of 150 rpm and pH of 7, (b) time dependent percentage removal expressed by $CoFe_2O_4$ towards PCG at solution concentration of 100 mg L^{-1}, speed of 150 rpm and pH of 7, (c) time dependent adsorption capacity expressed by $CoFe_2O_4$@MOF-5 towards PCG at solution concentration of 100 mg L^{-1}, speed of 150 rpm and pH of 7 and (d) time dependent percentage removal expressed by $CoFe_2O_4$@MOF-5 towards PCG at solution concentration of 100 mg L^{-1}, speed of 150 rpm and pH of 7.

PCG to the surfaces of $CoFe_2O_4$ and $CoFe_2O_4$@MOF-5. Interestingly, the crystallite sizes of $CoFe_2O_4$ and $CoFe_2O_4$@MOF-5 are smaller than those previously reported for ferrites [45]. The small sizes of $CoFe_2O_4$ and $CoFe_2O_4$@MOF-5 indicate that the adsorbates (MTZ and PCG) will migrate faster to their active site than the previously reported ferrites [45].

The thermal stability of $CoFe_2O_4$ and $CoFe_2O_4$@MOF-5 was studied by TGA (Fig. 1c). They were subjected to heating up to 800 °C while noting the degradation temperatures. The loss in weight at a temperature range of 50–162 °C in $CoFe_2O_4$ and $CoFe_2O_4$@MOF-5 was assigned to the loss of volatile and adsorbed water molecules (as seen in the FTIR peat at 3463 cm^{-1}). $CoFe_2O_4$@MOF-5 exhibited high weight loss at a temperature above 410 °C, which may be due to the decomposition of the organic framework [46]. Weight loss from 455 to 620 °C in both $CoFe_2O_4$ and $CoFe_2O_4$@MOF-5 may be attributed to the dehydration of OH groups in the spinel structure corresponding to intra and intermolecular transfer reactions and metal oxide formation phase [47,48]. Mass loss above 620 °C was attributed to the loss of the metal oxide phase. As shown in Fig. 1d, the EDS result confirmed the presence of Co, Fe and O as elemental composition of $CoFe_2O_4$ and $CoFe_2O_4$@MOF-5. Furthermore, C and Zn were established in $CoFe_2O_4$@MOF-5 due to the MOF-5 structure present in $CoFe_2O_4$@MOF-5. In both $CoFe_2O_4$ and $CoFe_2O_4$@MOF-5, the spectra revealed the presence of Cr due to coating the surfaces of $CoFe_2O_4$ and $CoFe_2O_4$@MOF-5 with Cr for high conductivity and improved imaging of the surfaces.

The BET surface area of $CoFe_2O_4$ is 16.63 m^2/g (Fig. 1e), and $CoFe_2O_4$@MOF-5 is 12.41 m^2/g (Fig. 1f). The surface area was reduced after the modification of $CoFe_2O_4$ with MOF-5 to form $CoFe_2O_4$@MOF-5. The reduction may be due to an increase in the crystallite size of $CoFe_2O_4$@MOF-5 which may have caused a reduction in the pore volume due to the incorporation of MOF-5 in the particles of $CoFe_2O_4$. In fact, the total pore volume of $CoFe_2O_4$ reduced from 0.143 $cm^3\ g^{-1}$ to 0.081 $cm^3\ g^{-1}$ ($CoFe_2O_4$@MOF-5) after the modification. Furthermore, the average pore diameter also decreased from 34.35 nm in $CoFe_2O_4$ to 26.10 nm in $CoFe_2O_4$@MOF-5, which clearly indicates the inclusion of MOF-5 in $CoFe_2O_4$ to form $CoFe_2O_4$@MOF-5. The pattern of the BET spectra is a typical of mesoporous adsorbent, a Type II BET isotherm [49]. The SEM image (Fig. 2a) and elemental surface mappings (Fig. 2bI-III) of $CoFe_2O_4$ further corroborate the EDS results for $CoFe_2O_4$. Similarly, the SEM image (Fig. 2c) and elemental surface mappings (Fig. 2dI-V) of $CoFe_2O_4$@MOF-5 additionally supports the EDS results for $CoFe_2O_4$@MOF-5. The SEM images revealed the surfaces of $CoFe_2O_4$ and $CoFe_2O_4$@MOF-5 to be heterogeneous with irregularly sized particles; however, a few of the particles on the surface of $CoFe_2O_4$ appeared spherical.

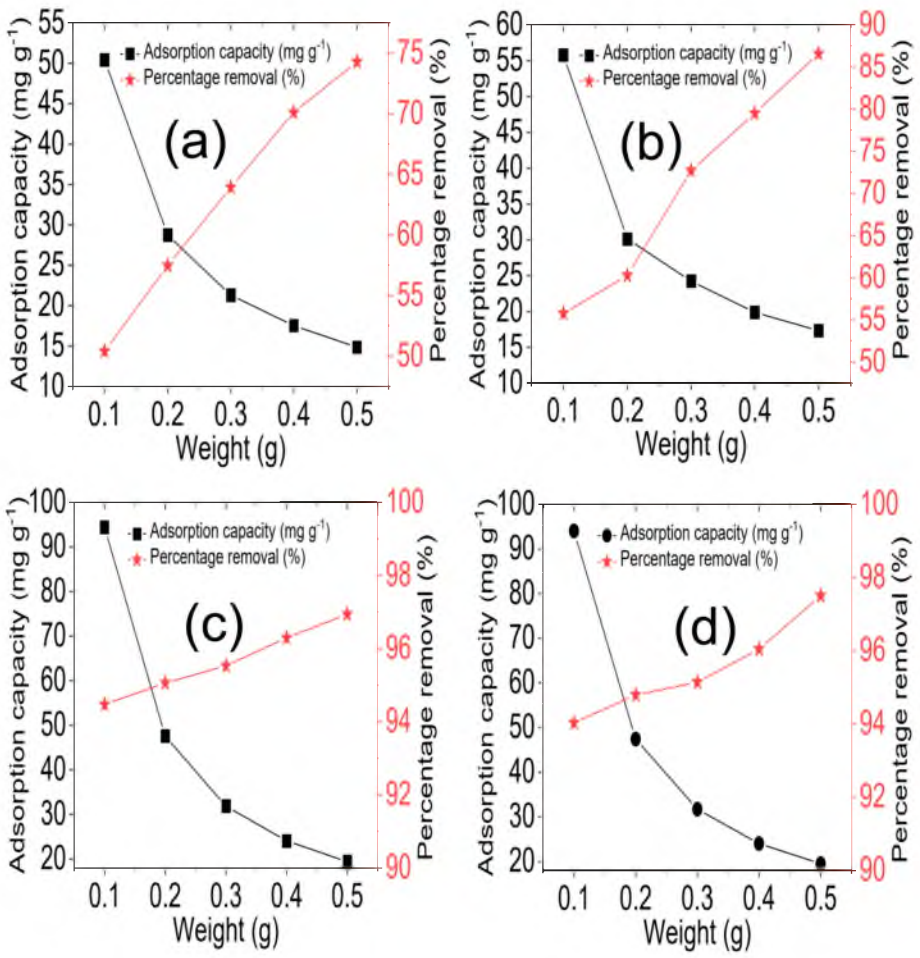

Fig. 5. Effect of weight of $CoFe_2O_4$ on adsorption capacity and percentage removal expressed towards MTZ (a), effect of weight of $CoFe_2O_4$ on adsorption capacity and percentage removal expressed towards PCG (b), effect of weight of $CoFe_2O_4$@MOF-5 on adsorption capacity and percentage removal expressed towards MTZ (c) and effect of weight of $CoFe_2O_4$@MOF-5 on adsorption capacity and percentage removal expressed towards PCG (d).

Adsorption of MTZ and PCG by $CoFe_2O_4$ and $CoFe_2O_4$@MOF-5

The adsorption capacity expressed by $CoFe_2O_4$ in removing MTZ from solution over 120 min is shown in Fig. 3a.

The capacity of $CoFe_2O_4$ increased gradually with time. The equilibrium adsorption capacity towards MTZ is 50.41 mg g^{-1} at a concentration of 100 mg L^{-1}. It was observed that the adsorption capacity increased as the concentration of MTZ in the solution increased, which may be due to the fact that as the concentration of MTZ increased, more species were available in the solution to interact with the surface of $CoFe_2O_4$. Therefore, there were more species of MTZ that $CoFe_2O_4$ could remove from the solution. On the contrary, the percentage removal expressed by $CoFe_2O_4$ towards MTZ increased with a decrease in concentration (Fig. 3b). The equilibrium percentage removal is 50.41 % at a concentration of 100 mg L^{-1} but increased to a 100 % removal at 5 mg L^{-1}. The observation may be due to the interaction of $CoFe_2O_4$ with a low amount of MTZ species in solution as concentration decreased. With a decrease in concentration (low amount of MTZ species in solution), the workload on $CoFe_2O_4$ became smaller, which made it possible for $CoFe_2O_4$ to attain a 100 % removal at 5 mg L^{-1}. A similar observation was obtained when $CoFe_2O_4$@MOF-5 was used (Fig. 3c and d); however, the adsorption capacity increased from 50.41 to 94.47 mg g^{-1} at 100 mg L^{-1} (Fig. 3c).

The time-dependent performance of $CoFe_2O_4$ and $CoFe_2O_4$@MOF-5 for the removal of PCG from the solution is presented in Fig. 4a to d. The performance is similar to the trend obtained for MTZ, i.e., the adsorption capacity increased over time. The higher the concentration, the higher the adsorption capacity for both $CoFe_2O_4$ and $CoFe_2O_4$@MOF-5. However, the adsorption capacity and percentage removal expressed by $CoFe_2O_4$@MOF-5 is higher than that of $CoFe_2O_4$, showing a better performance of modified $CoFe_2O_4$.

The effect of the weight of $CoFe_2O_4$ on the removal of MTZ (Fig. 5a) and PCG (Fig. 5b) revealed an adsorption capacity that increased with a reduction in weight and a percentage removal that increased with an increase in weight. Similarly, $CoFe_2O_4$@MOF-5 gave the same results with removing MTZ (Fig. 5c) and PCG (Fig. 5d), revealing an adsorption capacity that increased with reduction in weight $CoFe_2O_4$@MOF-5 and percentage removal that increased with increase in weight of $CoFe_2O_4$@MOF-5.

The increased percentage removal with increased weight may be due to the increased surface area, making more active sites available for interaction with MTZ or PCG. In tangent to this, there was a reduction in adsorption capacity with an increase in weight which may be explained mathematically as shown in Eq. (1d); as the weight increased, the denominator also increased, which reduced the overall performance determined. In both situations, $CoFe_2O_4$@MOF-5 exhibited better performance than $CoFe_2O_4$.

The effect of pH on the sorption process showed that the performance of $CoFe_2O_4$ and $CoFe_2O_4$@MOF-5 towards MTZ (Fig. 6a) and PCG (Fig. 6b) was best at neutral pH conditions. As pH increased towards neutrality (pH 7), the adsorption capacity and percentage removal expressed by $CoFe_2O_4$ and $CoFe_2O_4$@MOF-5 towards MTZ and PCG increased. The performance decreased as pH increased towards alkalinity. Previous studies have shown that pH plays a vital role in surface

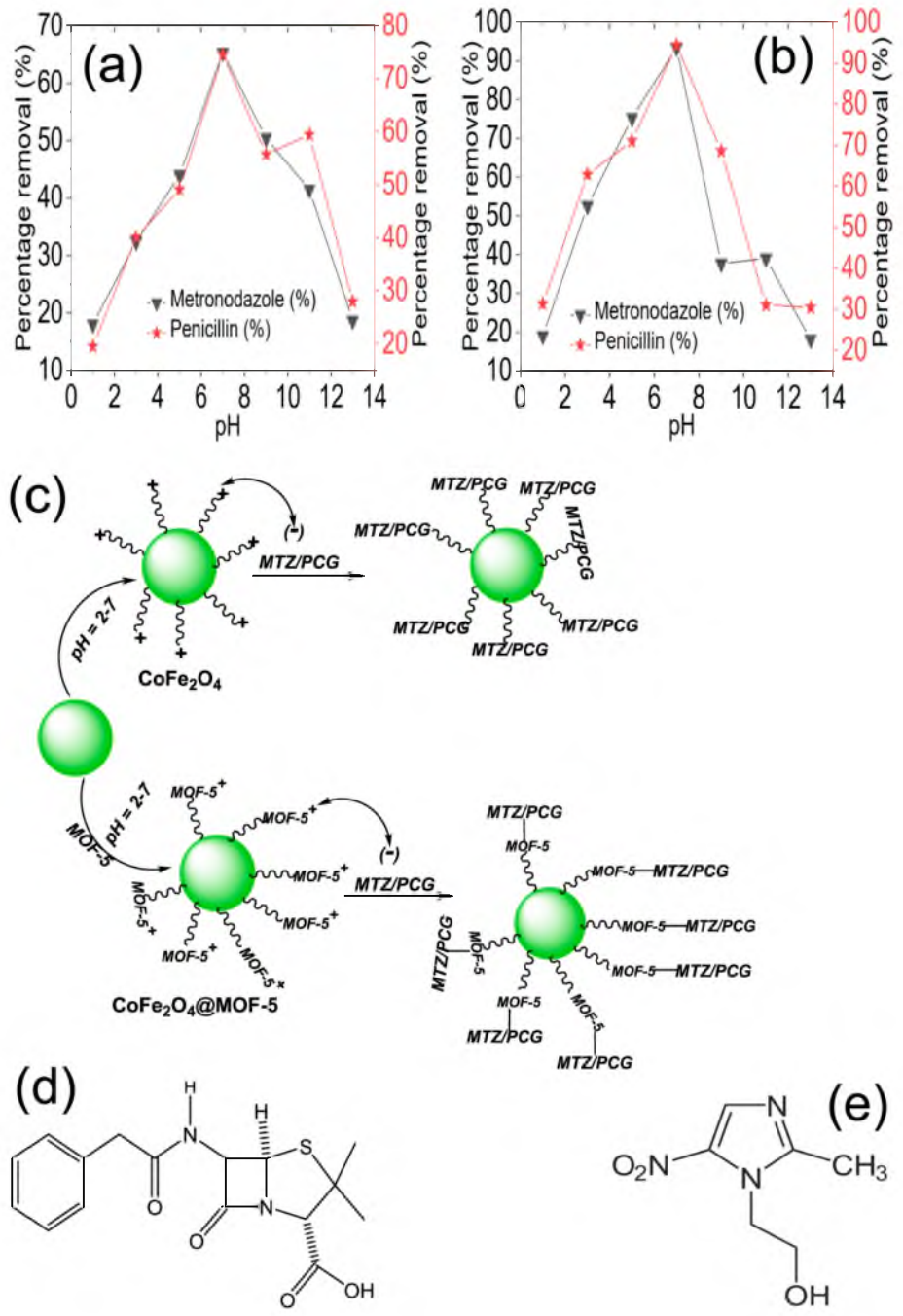

Fig. 6. Effect of pH change on the removal of MTZ and PCG by $CoFe_2O_4$ at concentration of 100 mg L^{-1}, weight of 0.1 g and speed of 150 rpm (a), effect of pH change on the removal of MTZ and PCG by $CoFe_2O_4$@MOF-5 at concentration of 100 mg L^{-1}, weight of 0.1 g and speed of 150 rpm (b), mechanism of removal of MTZ and PCG by $CoFe_2O_4$ and $CoFe_2O_4$@MOF-5 (c), structure of PCG (d) and structure of MTZ (e).

chemistry [30,50]. As the pH is within the acidic-neutral range, the surface of $CoFe_2O_4$ and $CoFe_2O_4$@MOF-5 becomes positively charged (protonated). This, as a result, promotes the interaction with the surfaces of MTZ and PCG, which are negatively charged as expressed below.

$$CoFe_2O_4@MOF\text{-}5 \rightarrow CoFe_2O_4@MOF\text{-}5^{+}\ pH \leq 7$$

$$CoFe_2O_4 \rightarrow CoFe_2O_4^{+}\ pH \leq 7$$

$$CoFe_2O_4@MOF\text{-}5^{+} + MTZ/PCG_{aq}^{-} \leftrightarrows CoFe_2O_4@MOF\text{-}5\text{-}MTZ/PCG + H^{+}$$

$$CoFe_2O_4^{+} + MTZ/PCG_{aq}^{-} \leftrightarrows CoFe_2O_4\text{-}MTZ/PCG + H^{+}$$

However, as pH moves from neutrality towards alkalinity (pH > 7), the surfaces of $CoFe_2O_4$ and $CoFe_2O_4$@MOF-5 become negatively (deprotonated) charge-repelling interaction with the surface of MTZ and PCG, which are negatively charged. This observation is expressed below.

$$CoFe_2O_4@MOF\text{-}5 \rightarrow CoFe_2O_4@MOF\text{-}5^{-}\ pH > 7$$

$$CoFe_2O_4 \rightarrow CoFe_2O_4^{-}\ pH > 7$$

$$CoFe_2O_4@MOF\text{-}5^{-} + MTZ/PCG_{aq}^{-} \leftrightarrows CoFe_2O_4@MOF\text{-}5^{-}\cdots MTZ/PCG^{-} + OH^{-}$$

$$CoFe_2O_4^{-} + MTZ/PCG_{aq}^{-} \leftrightarrows CoFe_2O_4^{-}\cdots MTZ/PCG^{-} + OH^{-}$$

The interaction between the surfaces of $CoFe_2O_4$ or $CoFe_2O_4$@MOF-5 and the MTZ or PCG may be described via electronic interaction. Electrons are promoted from the electron-rich centre (negatively

Table 1
Kinetic model parameters for the sorption of MTZ and PCG on $CoFe_2O_4$ and $CoFe_2O_4$@MOF-5.

Model	Parameter	$CoFe_2O_4$	$CoFe_2O_4$@MOF-5
MTZ			
Pseudo-First-order	q_e (mg g^{-1})	62.18	118.72
	k_1 (min^{-1})	1.68×10^{-4}	2.23×10^{-4}
	r^2	0.910	0.920
Pseudo-second-order	qe (mg g^{-1})	96.80	102.90
	k_2(g mg^{-1} min^{-1})	4.73×10^{-4}	5.54×10^{-5}
	r^2	0.930	0.970
Experiment	q_e (mg g^{-1})	50.41	94.47
PCG			
Pseudo-First-order	q_e (mg g^{-1})	80.80	93.35
	k_1 (min^{-1})	2.36×10^{-4}	1.61×10^{-4}
	r^2	0.842	0.950
Pseudo-second-order	qe (mg g^{-1})	120.40	102.85
	k_2(g mg^{-1} min^{-1})	3.53×10^{-4}	5.83×10^{-5}
	r^2	0.952	0.972
Experiment	q_e (mg g^{-1})	55.76	90.28

Table 2
MTZ and PCG sorption parameters for Langmuir and Freundlich models.

Isotherm	$CoFe_2O_4$	$CoFe_2O_4$@MOF-5
MTZ		
Langmuir		
Q_o (mg g^{-1})	54.65	104.17
K_L (L mg^{-1})	0.511	0.110
r^2	0.984	0.999
R_L	0.010	0.010
Freundlich		
K_f (L mg^{-1})	2.34	1.16
1/n	0.949	2.320
r^2	0.927	0.900
PCG		
Langmuir		
Q_o (mg g^{-1})	53.48	100.01
K_L (L mg^{-1})	1.00	0.362
r^2	0.920	0.980
R_L	0.020	0.027
Freundlich		
K_f (L mg^{-1})	9.927	5.21
1/n	1.79	1.01
r^2	0.940	0.992

charged MTZ/PCG) to the electron-deficient centre (positively charged $CoFe_2O_4$ and $CoFe_2O_4$@MOF-5) to form covalent bond promoting the removal of MTZ or PCG from solution at pH $\leq$ 7. The electronic interaction mechanism for removing MTZ or PCG by $CoFe_2O_4$ and $CoFe_2O_4$@MOF-5 is described in Fig. 6c.

Table 3
ΔG and q_e obtained at various temperatures for the sorption of MTZ and PCG by $CoFe_2O_4$.

MTZ					
T (K)	303	308	313	318	323
qe (mg g^{-1})	50.41	53.59	64.65	66.24	74.65
ΔG (kJ mol^{-1} K^{-1})	−0.041	−0.368	−1.570	−1.782	−2.900
PCG					
T (K)	303	308	313	318	323
qe (mg g^{-1})	55.76	65.07	72.78	74.93	86.60
ΔG (kJ mol^{-1} K^{-1})	−3.180	−4.770	−6.960	−7.900	−17.350

Table 4
ΔG and q_e obtained at various temperatures for the sorption of MTZ and PCG by $CoFe_2O_4$@MOF.

MTZ					
T (K)	303	308	313	318	323
qe (mg g^{-1})	94.47	95.00	95.41	96.24	97.71
ΔG (kJ mol^{-1} K^{-1})	−7.150	−7.540	−7.897	−8.577	−10.075
PCG					
T (K)	303	308	313	318	323
qe (mg g^{-1})	90.28	94.03	95.28	96.60	98.75
ΔG (kJ mol^{-1} K^{-1})	5.614	7.059	7.819	8.846	11.734

Table 5
ΔS° and ΔH° values for the sorption of MTZ and PCG by $CoFe_2O_4$ and $CoFe_2O_4$@MOF-5.

Isotherm	$CoFe_2O_4$	$CoFe_2O_4$@MOF-5
MTZ		
ΔS° (kJ mol^{-1})	142.23	135.97
ΔH° (kJ mol^{-1} K^{-1})	−43.18	−3.51
PCG		
ΔS° (kJ mol^{-1})	202.1383	278.59
ΔH° (kJ mol^{-1} K^{-1})	60.74	−78.98

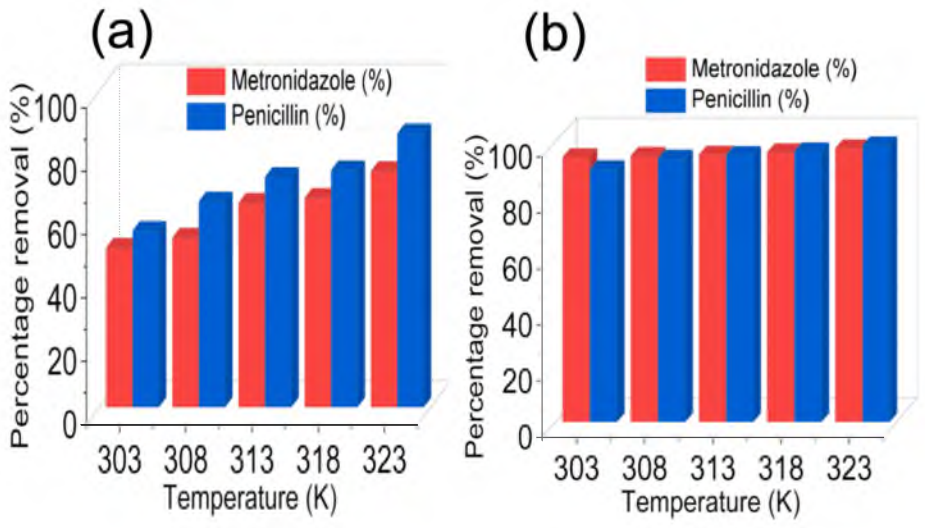

Fig. 7. Effect of temperature change on the removal of MTZ and PCG by $CoFe_2O_4$ at concentration of 100 mg L^{-1}, weight of 0.1 g and speed of 150 rpm (a) and effect of temperature change on the removal of MTZ and PCG by $CoFe_2O_4$@MOF-5 at concentration of 100 mg L^{-1}, weight of 0.1 g and speed of 150 rpm (b).

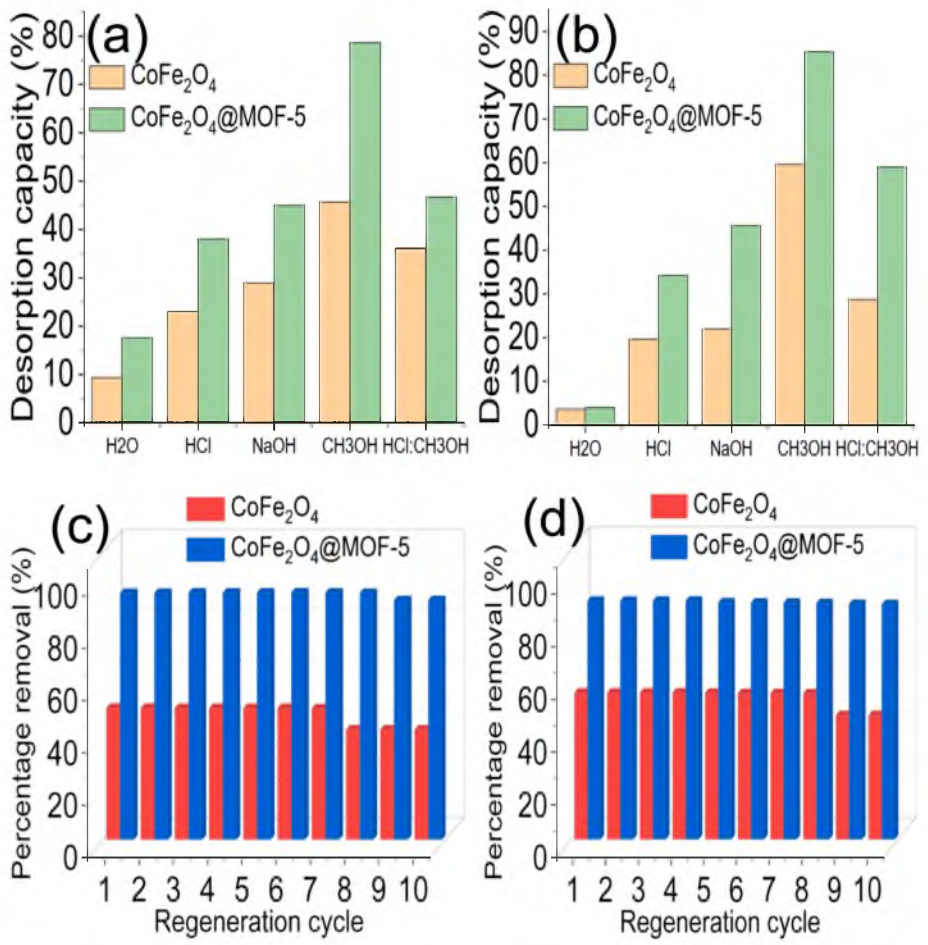

Fig. 8. Desorption of MTZ from the surface of $CoFe_2O_4$ and $CoFe_2O_4$@MOF-5 (a), desorption of PCG from the surface of $CoFe_2O_4$ and $CoFe_2O_4$@MOF-5 (b), regeneration capacity expressed by $CoFe_2O_4$ and $CoFe_2O_4$@MOF-5 for MTZ (c) and regeneration capacity expressed by $CoFe_2O_4$ and $CoFe_2O_4$@MOF-5 for PCG (d).

Process kinetic and isotherm fittings

The data generated were fitted for pseudo 1st and 2nd order kinetics as determined from adsorption capacities of $CoFe_2O_4$ and $CoFe_2O_4$@-MOF-5 at time t and equilibrium, represented as q_t (mg/g) and q_e (mg/g), respectively. The pseudo 1st and 2nd order kinetics rate constants are k_1 (min^{-1}) and k_2 (g mg^{-1} min^{-1}), respectively, while time is given as t. The pseudo-1st-order was estimated using Eq. (7):

$$log(q_e - q_t) = \log q_e - \frac{k_1}{2.303} t \tag{7}$$

while the pseudo-2nd-order was determined from Eq. (8):

$$\frac{t}{q_t} = \frac{1}{k_2 q_e^2} + \frac{1}{q_e} t \tag{8}$$

The value of k_1 was determined by plotting ln (q_e-q_t) against t for the pseudo-1st-order kinetic, while k_2 was determined by plotting $\frac{t}{q_t}$ against t for the pseudo-2nd-order kinetic. The k_1 values for the sorption of MTZ by $CoFe_2O_4$ and $CoFe_2O_4$@MOF-5 were found to be 1.86×10^{-4} and 2.23×10^{-4} min^{-1}, respectively, while the k_2 values for the sorption of MTZ by $CoFe_2O_4$ and $CoFe_2O_4$@MOF-5 are 4.73×10^{-4} and 5.54×10^{-5} g mg^{-1} min^{-1}, respectively as shown in Table 1. The higher value of k_1 for $CoFe_2O_4$@MOF-5 suggests a faster sorption process of MTZ than when $CoFe_2O_4$ was used. On the contrary, the k_2 value is higher for $CoFe_2O_4$ than for $CoFe_2O_4$@MOF-5, which suggests a faster sorption process of MTZ for $CoFe_2O_4$. For the sorption of PCG, the k_1 values for $CoFe_2O_4$ and $CoFe_2O_4$@MOF-5 were found to be 2.36×10^{-4} and 1.61×10^{-4} min^{-1}, respectively, while the k_2 values were 3.53×10^{-4} and 5.83×10^{-5} g mg^{-1} min^{-1}, respectively. Results for other parameters are also presented in Table 1.

Data were further subjected for Langmuir and Freundlich isotherms using the equilibrium concentration of MTZ and PCG as C_e (mg L^{-1}) and the adsorption capacity of $CoFe_2O_4$ and $CoFe_2O_4$@MOF-5 at equilibrium as q_e (mg g^{-1}). The Langmuir isotherm was expressed as previously described [51]:

$$\frac{C_e}{q_e} = \frac{1}{Q_o} C_e + \frac{1}{Q_o K_L} \tag{9}$$

The maximum monolayer coverage, Q_o (mg g^{-1}) and Langmuir isotherm constant, K_L (L mg^{-1}), was calculated from the plot of C_e/q_e *vs* Ce. The Q_o (54.65 mg g^{-1}) exhibited by $CoFe_2O_4$ for the sorption of MTZ is closely related to the experimental adsorption capacity value of 50.41 g g^{-1} at an r^2 value of 0.984, suggesting that the process can be described by Langmuir isotherm. Furthermore, the Q_o exhibited by $CoFe_2O_4$@MOF-5 is 104.17 mg g^{-1}, which is not far from the experimental adsorption capacity of 94.47 mg g^{-1} at an r^2 value of 0.999. The results suggest that the process may be described by Langmuir isotherm. The R_L values for the sorption process were determined from the initial concentration (C_o, mg L^{-1}) of MTZ and PCG and the Langmuir constant, which is related to the energy given as K_L in the expression given in Eq. (10).

$$R_L = \frac{1}{1 + K_L C_o} \tag{10}$$

A previous study has shown that when the value of R_L is $R_L > 1$, the process becomes unfavourable; when the value of $R_L = 1$, the process is

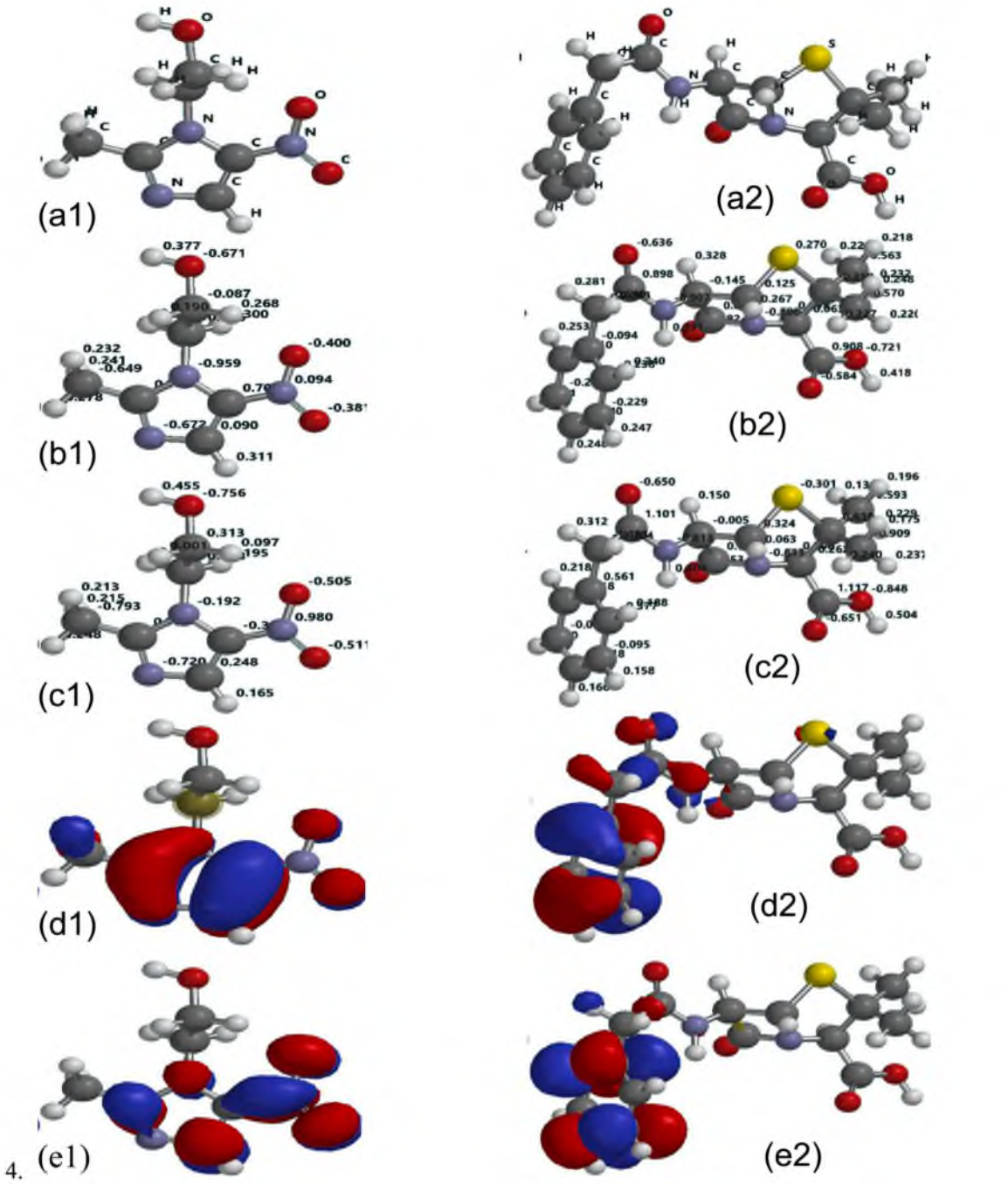

Fig. 9. Electronic properties of MTZ and PCG: Optimized geometry of MTZ (a1) and PCG (a2); Mulliken charge of MTZ (b1), and PCG (b2); electrostatic charge of MTZ (c1), and PCG (c2); highest occupied molecular orbital of MTZ (d1), and PCG (d2) and lowest unoccupied molecular orbital of MTZ (e1), and PCG (e2).

taken to be linear, and when $0 < R_L < 1$, the process is favourable; furthermore, when the value is $R_L = 0$, then the process becomes irreversible [30]. The values of R_L obtained in this study fall within the range of $0 < R_L < 1$, suggesting the sorption process is Langmuir isotherm favoured. The implication of this is that the sorption process of MTZ and PCG by $CoFe_2O_4$ and $CoFe_2O_4$@MOF-5 occurred by a monolayer interaction without interaction between the molecules of MTZ or PCG. Conformity with Freundlich isotherm was checked by subjecting data to Eq. (11):

$$q_e = K_F C_e^{1/n} \tag{11}$$

The parameters for Freundlich isotherm were obtained from the plot of ln q_e *vs* ln C_e. As shown in Table 2, the r^2 values obtained for the sorption of MTZ by $CoFe_2O_4$ (0.927) and $CoFe_2O_4$@MOF-5 (0.900) and the sorption of PCG by $CoFe_2O_4$ (0.940) and $CoFe_2O_4$@MOF-5 (0.992) showed that the process could be described by Freundlich isotherm suggesting the surfaces to be heterogeneous [52]. It may be inferred that the sorption of MTZ and PCG by $CoFe_2O_4$ may be described by both Langmuir and Freundlich isotherms; likewise, the sorption of MTZ and PCG by $CoFe_2O_4$@MOF-5 may be described by both Langmuir and Freundlich isotherms. This means that both monolayer adsorption and multilayer adsorption occurred during the sorption process of MTZ and PCG by $CoFe_2O_4$ and $CoFe_2O_4$@MOF-5. From the Freundlich parameter, the 1/n plays an essential role in describing the process; when $1/n = 1$, the sorption process is independent of the concentration of pollutants in the solution; when $1/n < 1$, the sorption is determined to be normal, and the process is cooperative adsorption when $1/n > 1$ [38]. The value of 1/

Table 6
Molecular properties of MTZ and PCG calculated using DFT at B3LYP/6-31G basis set level.

Quantum Chemical Property	MTZ	PCG
Molecular surface area (Å^2)	185.57	342.01
Energy (au)	−616.75	−1414.72
E_{HOMO} (eV)	−9.89	−9.36
E_{LUMO} (eV)	1.08	3.56
$E_{LUMO-HOMO}$ (eV)	10.97	12.92
Dipole moment (D)	6.01	4.20
Volume (Å^3)	158.74	318.48
Solvation energy (kJ mol^{-1})	−54.06	−45.17
Group	*C1*	*C1*
Polarizability	51.67	64.17
η (eV)	5.49	6.46

n for the sorption of MTZ by $CoFe_2O_4$ falls within $1/n < 1$, indicating a normal adsorption process, whereas the values for the sorption of MTZ and PCG by $CoFe_2O_4$@MOF-5 and sorption of PCG by $CoFe_2O_4$ falls within $1/n > 1$ suggesting the sorption process to be cooperative.

Thermodynamic parameter for the sorption of MTZ and PCG by $CoFe_2O_4$ and $CoFe_2O_4$@MOF-5

The impact of temperature on the adsorption of MTZ and PCG by $CoFe_2O_4$ and $CoFe_2O_4$@MOF-5 is shown in Fig. 7a and b.

The removal of MTZ and PCG by $CoFe_2O_4$ and $CoFe_2O_4$@MOF-5 increased with a rise in temperature from 303 to 323 K. An increase in temperature enhances the sorption process. This observation may be because as temperature increased, the average kinetic energy for the molecules of MTZ and PCG increased, facilitating their movements towards the surface of $CoFe_2O_4$ and $CoFe_2O_4$@MOF-5 for interaction. $CoFe_2O_4$ showed better removal capacity for PCG than MTZ, which might be due to the fact that there is a more different possible point of interaction (lone pairs of electrons from the heteroatoms) on PCG (Fig. 6d) than MTZ (Fig. 6e). There are more heteroatoms that may be involved in bonding in PCG than in MTZ. Similarly, with increased temperature, $CoFe_2O_4$@MOF-5 exhibited higher removal capacity towards PCG than MTZ. The adsorption capacity also increased with temperature (Tables 3 and 4).

From the equilibrium capacity, q_e (mg g^{-1}), equilibrium concentration, C_e (mg L^{-1}), temperature, T (K) and gas constant, R (8.314 J mol^{-1} K^{-1}), the entropy change (ΔS°), enthalpy change (ΔH°), and process equilibrium constant (b_o) were determined from the following equations.

$$b_o = \frac{q_e}{C_e} \tag{12}$$

$$\Delta G^o = -RTlnb_o \tag{13}$$

$$\Delta G^o = \Delta H^o - T\Delta S^o \tag{14}$$

The ΔG° values calculated for the processes are negative, suggesting the processes are spontaneous, except for the sorption of PCG by $CoFe_2O_4$@MOF-5, which is positive, suggesting a nonspontaneous process. The plot of ln *bo vs* 1/T was evaluated to determine the values of ΔH^o and ΔS^o for the sorption of MTZ and PCG by $CoFe_2O_4$ and $CoFe_2O_4$@MOF-5 (Table 5). The ΔH^o values for the sorption of MTZ by $CoFe_2O_4$ (−43.18 kJ mol^{-1} K^{-1}) and $CoFe_2O_4$@MOF-5 (−3.51 kJ mol^{-1} K^{-1}) are negative, suggesting the process to be exothermic, a similar observation was noted for the sorption of PCG by $CoFe_2O_4$@MOF-5 except for the sorption of PCG by $CoFe_2O_4$ which is positive suggesting and endothermic process. The ΔS° value for the sorption process is positive, suggesting an increased disordered configuration of MTZ and PCG on the surfaces of $CoFe_2O_4$ and $CoFe_2O_4$@MOF-5.

Desorption and regeneration studies

The desorption of MTZ (Fig. 8a) and PCG (Fig. 8b) from the surface of $CoFe_2O_4$ and $CoFe_2O_4$@MOF-5 was determined using different solvents. The best desorption capacity was obtained when CH_3OH was used. The MTZ and PCG desorbed better from the surface of $CoFe_2O_4$@MOF-5 than $CoFe_2O_4$. A desorption capacity of 78.65 % was obtained for removing MTZ from the surface of $CoFe_2O_4$@MOF-5 and 45.71 % from the surface of $CoFe_2O_4$. Furthermore, the desorption of PCG from the surface of $CoFe_2O_4$@MOF-5 was 85.35 %, while that of $CoFe_2O_4$ was 59.65 %. The surface of $CoFe_2O_4$@MOF-5 and $CoFe_2O_4$ were regenerated in 10 cycles of operation to determine capacity for reuse. The value revealed a consistent regeneration of the surfaces with $CoFe_2O_4$@MOF-5 exhibiting a better performance when compared with $CoFe_2O_4$. The regeneration capacity exhibited by $CoFe_2O_4$ at the 10th cycle of operation towards

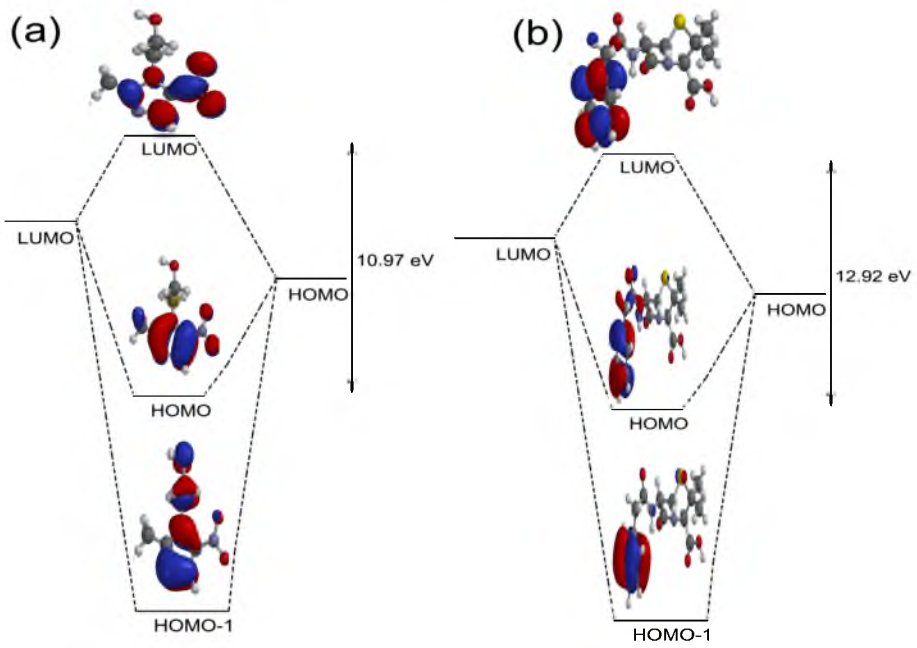

Fig. 10. Molecular orbitals of MTZ (a) and PCG (b).

Table 7
Comparison of the adsorption of MTZ and PCG on $CoFe_2O_4$ and $CoFe_2O_4$@MOF-5 with other adsorbents in literature.

Material	Adsorbate	q_e (mg g^{-1})	Adsorption isotherm	$\Delta G°_{ads}$ (kJ/mol)	$\Delta H°_{ads}$ (kJ/mol)	% removal	Desorption (%)	Reference
$FeNi_3/SiO_2/CuS$	MTZ	135.14	Langmuir	−19.88	+0.06	85.26	53.97 (5th cycle)	[27]
MAC	MTZ	66.22	Freundlich	–	–	95.00	73.00 (5th cycle)	[61]
Plantain wood	MTZ	11.38	Langmuir	–	+11.69	91.00	–	[62]
CF/AC@Ch	MTZ	35.9	Freundlich	–	–	55.00	–	[63]
CS-GO	MTZ	29.76	Langmuir	–	–	–	–	[64]
Rice husk ash	MTZ	39.00	Langmuir	−759.10	+1.83	76.47	–	[59]
PPY-PANi	MTZ	63.84	Freundlich	− 7.47	− 37.32	89.24	–	[65]
CTN-HNT	MTZ	15.80	Langmuir	–	–	63.19	–	[66]
Graphene oxide	MTZ	75.22	Langmuir	−0.346	32.86	–	–	[58]
MWCNT	MTZ	4.80	Freundlich	122.45	59.87	–	–	[60]
Duckweed	PCG	36.18	Langmuir	–	–	94.60	–	[67]
HDTMA-Mt	PCG	88.5	Freundlich	0.54	13.09	–	–	[68]
MgO	PCG	25.66	Langmuir & Freundlich	–	–	80.00	–	[69]
Chitosan	PCG	101.44	Langmuir	–	5.69	–	–	[70]
CuO-NPs	PCG	15.00	–	–	–	83.00	–	[71]
TiO_2 nanotubes	PCG	35.58	Langmuir	–	–	–	–	[72]
Activated carbon	PCG	8.41	Langmuir & Freundlich	−58.51	55.70	69.48	32.98 (4th cycle)	[73]
$CoFe_2O_4$	MTZ	50.41	Langmuir & Freundlich	−41.49	−43.18	50.41	42.18 (10th cycle)47.22	This study
	PCG	55.76	Langmuir	−3.18	60.74	55.76	(10th cycle)	
$CoFe_2O_4$@MOF-5	MTZ	94.47	Langmuir	−7.15	−3.51	94.47	91.71 (10th cycle)89.31	This study
	PCG	90.28	Langmuir & Freundlich	5.61	−78.98	90.28	(10th cycle)	

– = Not reported.
modified activated carbon = MAC, Multi-Walled Carbon Nanotube = MWCNTs, $CoFe_2O_4$/Activated Carbon@Chitosan = CF/AC@Ch, chitosan-modified graphene oxide = CS–GO, polyaniline-polypyrrole (PPY-PANi) = PPY-PANi, CTN-HNT = chitosan and halloysite nanotubes, Hexadecyl Trimethyl Ammonium Bromide modified montmorillonite = HDTMA-Mt.

MTZ was 42.18 % and 47.22 % towards PCG. In comparison, $CoFe_2O_4$@MOF-5 demonstrated 91.71 % towards MTZ and 89.31 % towards PCG, as shown in Fig. 8c and Fig. 8d. These results revealed the stability of $CoFe_2O_4$@MOF-5 as a promising material for the removal of MTZ and PCG from the contaminated water system.

Quantum chemical simulation

The sorption of MTZ and PCG by $CoFe_2O_4$ and $CoFe_2O_4$@MOF-5 was subjected to quantum computational analysis to understand the electronic interaction leading to the sorption. The interaction was investigated by considering the electronic properties of MTZ and PCG (Fig. 9). The geometry of MTZ and PCG revealed that they contain oxygen, nitrogen and sulphur as heteroatoms (Fig. 9a1 and a2) with nonbonding electrons that can take part in electronic bonding with the orbitals of $CoFe_2O_4$ and $CoFe_2O_4$@MOF-5. Furthermore, the Mulliken (Fig. 9b1 and b2) and electrostatic charges (Fig. 9c1 and c2) revealed some negative charges, which corroborates the presence of nonbonding electrons in their structure. These negative charges represent electrons that may be donated to the vacant orbitals of $CoFe_2O_4$ or $CoFe_2O_4$@MOF-5 for bonding which may include the d-orbitals to drive the adsorption process.

The molecular properties (Table 6) revealed E_{HOMO} to −9.89 and −9.36 eV for MTZ and PCG, respectively. At the same time, the E_{LUMO} are 1.08 and 3.56 eV, respectively, suggesting that the reactivity of MTZ and PCG may be related to the frontier molecular orbitals (HOMO and LUMO) and their respective energies [31]. The dipole moment may help understand the non-uniform distribution of charges in MTZ and PCG. Intermolecular attraction increases as the dipole moment increases [30]. In this study, the dipole moment of MTZ (6.01 D) and PCG (4.20 D) is higher than that of water (1.85 D) previously reported [53], suggesting a promising interaction of MTZ and PCG with the surfaces of $CoFe_2O_4$ and $CoFe_2O_4$@MOF-5. The relationship may be related to the adsorption susceptibility of MTZ and PCG [54,55]. Molecules with high polarizability have high reactivity and low kinetic stability; they are also referred to as being soft [56,57]. The polarizability of PCG is higher than that of MTZ. This might be the reason for the higher adsorption capacity expressed towards PCG, and the low kinetic stability may also be a reason for its better desorption capacity when compared to MTZ.

In the case of MTZ, the electron density is mostly concentrated on the nitrogen and the ring structure for the HOMO (Fig. 9d1), while in the LUMO (Fig. 9e1), the electron density is concentrated on oxygen and nitrogen atoms. For the PCG, the electron density is concentrated on the oxygen, sulphur, nitrogen and the benzene ring for the HOMO (Fig. 9d2), while for its LUMO (Fig. 9e2), the electrons are concentrated mainly on the benzene ring. Electrons can be transferred from the densely concentrated region to the unoccupied d-orbitals in $CoFe_2O_4$ and $CoFe_2O_4$@MOF-5 for bonding. As a result, the sorption of MTZ and PCG from the solution becomes possible. Moreover, a back-donating bond may also be formed to remove MTZ and PCG from the solution; when this occurs, electrons are donated from the anti-bonding orbitals of $CoFe_2O_4$ or $CoFe_2O_4$@MOF-5 to the molecules of MTZ and PCG. In corroborating this, the frontier molecular orbital of MTZ and PCG are presented in Fig. 10, revealing the HOMO and LUMO electronic interaction possibilities for the sorption process.

The performance of $CoFe_2O_4$ and $CoFe_2O_4$@MOF-5 for the removal of MTZ and PCG from the are further compared with other results from the literature in Table 7. $CoFe_2O_4$@MOF-5 performed better than $CoFe_2O_4$, suggesting the important role of MOF-5 in improving $CoFe_2O_4$ performance for the MTZ and PCG removal. Similarly, $CoFe_2O_4$@MOF-5 compared favourably with most adsorbents in the solution. The adsorption capacity of $CoFe_2O_4$@MOF-5 is higher than the capacity expressed by graphene oxide [58], rice husk ash [59] and MWCNT [60] towards MTZ. On the contrary, $FeNi_3/SiO_2/CuS$ [27] showed higher adsorption capacity than $CoFe_2O_4$@MOF-5.

However, despite the higher adsorption capacity of $FeNi_3/SiO_2/CuS$, $CoFe_2O_4$@MOF-5 demonstrated a higher percentage removal (94.47 %) than $FeNi_3/SiO_2/CuS$ (85.26 %). Furthermore, $CoFe_2O_4$@MOF-5 exhibited a higher stability from its regeneration capacity of 91.71 % at its 10th cycle of operation, unlike $FeNi_3/SiO_2/CuS$, which could only attain 53.97 % at its 5th cycle of operation. Regarding PCG, $CoFe_2O_4$@MOF-5 performed better than activated carbon [73], MgO [69] and TiO_2 nanotubes [72]. The adsorption process demonstrated by $CoFe_2O_4$@MOF-5 for removing MTZ may be described by Langmuir isotherm. Similarly, most adsorbent previously reported demonstrated processes that could be described by Langmuir isother except MAC [61], CF/AC@Ch [63] and PPY-PANi [65] which obeys Freundlich isotherms. On the other hand, the interaction of $CoFe_2O_4$@MOF-5 with PCG may be

described by Langmuir and Freundlich isotherms. Likewise, the interaction of activated carbon [73] and MgO [69] with PCG may also be described by Langmuir and Freundlich isotherms. The performance exhibited by $CoFe_2O_4$@MOF-5 showed that it is a promising adsorbent for removing MTZ and PCG from the solution.

Conclusion

Water pollution by antibiotics such as MTZ and PCG is a serious concern. Many methods have been developed to circumvent the problem, but the major drawback has been inefficient removal and poor reusability. Therefore, this study improved the capacity of $CoFe_2O_4$ as an adsorbent by modification forming $CoFe_2O_4$@MOF-5 to remove MTZ and PCG from aqueous solutions. $CoFe_2O_4$ and $CoFe_2O_4$@MOF-5 were characterized with FTIR, SEM, EDS, XRD, TGA and BET. The BET surface area was 16.63 and 12.41 m^2/g for $CoFe_2O_4$ and $CoFe_2O_4$@MOF-5, respectively. The XRD revealed a crystallite size of 28.31 nm for $CoFe_2O_4$ and 29.01 nm for $CoFe_2O_4$@MOF-5. The SEM results showed the surfaces to be heterogeneous with irregularly shaped particles, while the elemental composition was confirmed using EDS. $CoFe_2O_4$@MOF-5 exhibited higher sorption capacity towards MTZ (94.47 mg g^{-1}) and PCG (90.28 mg g^{-1}) than values exhibited by $CoFe_2O_4$ towards MTZ (50.41 mg g^{-1}) and PCG (55.76 mg g^{-1}). Langmuir and Freundlich isotherms may describe the sorption process with a process mechanism of electronic interaction. The performance of $CoFe_2O_4$ and $CoFe_2O_4$@-MOF-5 is pH dependent. The regeneration capacity of $CoFe_2O_4$@MOF-5 is higher than that of $CoFe_2O_4$, with a regeneration capacity of 91.71 % for MTZ and 89.31 % for PCG at the 10th regeneration cycle. The study's findings revealed $CoFe_2O_4$@MOF-5 as a promising material for the purification of water contaminated with MTZ and PCG.

Funding

The research did not receive any fund of any form.

CRediT authorship contribution statement

Babatunde K. Adeleke: Investigation, Visualization, Formal analysis. **Olamide A. Olalekan:** Investigation, Formal analysis. **Adewale Adewuyi:** Conceptualization, Formal analysis, Investigation, Writing – original draft, Writing – review & editing, Visualization. **Woei Jye Lau:** Formal analysis, Investigation, Writing – original draft, Writing – review & editing, Visualization. **Olalere G. Adeyemi:** Conceptualization, Formal analysis, Investigation, Writing – original draft, Writing – review & editing.

Declaration of Competing Interest

The authors declare that they have no known competing financial interests or personal relationships that could have appeared to influence the work reported in this paper.

Data availability

Data will be made available on request.

Acknowledgement

Authors are grateful to the Department of Chemical Sciences, Redeemer's University, Nigeria for provision of research space and chemicals. The support received from Department of Chemistry, University of Cambridge, UK is highly appreciated.

References

[1] S.I. Polianciuc, A.E. Gurzău, B. Kiss, M.G. Ştefan, F. Loghin, Antibiotics in the environment: causes and consequences, Med. Pharm. Rep. 93 (2020) 231.
[2] D.J. Larsson, C.-F. Flach, Antibiotic resistance in the environment, Nat. Rev. Microbiol. 20 (2022) 257–269.
[3] Y. Kuang, X. Guo, J. Hu, S. Li, R. Zhang, Q. Gao, X. Yang, Q. Chen, W. Sun, Occurrence and risks of antibiotics in an urban river in northeastern Tibetan Plateau, Sci. Rep. 10 (2020) 1–11.
[4] R. Singh, A.P. Singh, S. Kumar, B.S. Giri, K.-H. Kim, Antibiotic resistance in major rivers in the world: a systematic review on occurrence, emergence, and management strategies, J. Clean. Prod. 234 (2019) 1484–1505.
[5] C. Uluseker, K.M. Kaster, K. Thorsen, D. Basiry, S. Shobana, M. Jain, G. Kumar, R. Kommedal, I. Pala-Ozkok, A review on occurrence and spread of antibiotic resistance in wastewaters and in wastewater treatment plants: mechanisms and perspectives, Front. Microbiol. 12 (2021), 717809.
[6] D. Rodríguez-Molina, P. Mang, H. Schmitt, M.C. Chifiriuc, K. Radon, L. Wengenroth, Do wastewater treatment plants increase antibiotic resistant bacteria or genes in the environment? Protocol for a Systematic Review, System. Rev. 8 (2019) 304.
[7] J. Lyu, Y. Chen, L. Zhang, Antibiotics in Drinking Water and Health Risks—China, 2017, China CDC Weekly, 2 (2020) 413.
[8] M. Aram, M. Farhadian, A.R.S. Nazar, S. Tangestaninejad, P. Eskandari, B.-H. Jeon, Metronidazole and Cephalexin degradation by using of Urea/TiO2/ZnFe2O4/Clinoptiloite catalyst under visible-light irradiation and ozone injection, J. Mol. Liq. 304 (2020), 112764.
[9] A. Cizek, M. Masarikova, J. Mares, M. Brajerova, M. Krutova, S. Bekal, Detection of plasmid-mediated resistance to metronidazole in Clostridioides difficile from river water, Microbiol. Spectrum 10 (4) (2022).
[10] D. Li, M. Yang, J. Hu, Y. Zhang, H. Chang, F. Jin, Determination of penicillin G and its degradation products in a penicillin production wastewater treatment plant and the receiving river, Water Res. 42 (2008) 307–317.
[11] S.A. Dingsdag, N. Hunter, Metronidazole: an update on metabolism, structure–cytotoxicity and resistance mechanisms, J. Antimicrob. Chemother. 73 (2018) 265–279.
[12] A.H. Ceruelos, L. Romero-Quezada, J.R. Ledezma, L.L. Contreras, Therapeutic uses of metronidazole and its side effects: an update, Eur. Rev. Med. Pharmacol. Sci. 23 (2019) 397–401.
[13] R. Iyer, Beta Lactam, Comprehensive, Pharmacology (2022) 3–63.
[14] A. Hossain, S. Nakamichi, M. Habibullah-Al-Mamun, K. Tani, S. Masunaga, H. Matsuda, Occurrence and ecological risk of pharmaceuticals in river surface water of Bangladesh, Environ. Res. 165 (2018) 258–266.
[15] Q. Wu, X. Zhao, S. Peng, L. Wang, X. Zhao, Risk Assessment and effect of Penicillin-G on bacterial diversity in drinking water, IOP Conf. Ser.: Earth Environ. Sci., IOP Publishing 113 (2018), 012156.
[16] W. Du, H. Zhou, Z. Luo, P. Zheng, P. Guo, R. Chang, C. Chang, Q. Fu, Selective determination of penicillin G from tap water and milk samples using surface molecularly imprinted polymers as solid-phase extraction sorbent, Molecular Imprinting 2 (2014) 18–29.
[17] A. Adewuyi, F.V. Pereira, Preparation and application of EDTA-functionalized underutilized Adansonia digitata seed for removal of Cu (II) from aqueous solution, Sustainable Environ. Res. 28 (3) (2018) 111–120.
[18] Z.Z. Chowdhury, K. Pal, S. Sagadevan, W.A. Yehye, R.B. Johan, S.T. Shah, A. Adebesi, M.E. Ali, M.S. Islam, R.F. Rafique, Electrochemically active carbon nanotube (CNT) membrane filter for desalination and water purification, Emerging Technologies for Sustainable Desalination Handbook, Elsevier2018, pp. 333-363.
[19] A.J. Campbell, O.A. Olalekan, J.O. Origomisan, A. Adewuyi, W.J. Lau, O. G. Adeyemi, Synthesis and Application of SeFe2O4@ Cell for the Removal of Polyethylene glycol from Aqueous Solution, Environmental Nanotechnology, Monitor. Manage. 20 (2023), 100802.
[20] H. Wang, X. Lou, Q.i. Hu, T. Sun, Adsorption of antibiotics from water by using Chinese herbal medicine residues derived biochar: Preparation and properties studies, J. Mol. Liq. 325 (2021), 114967.
[21] M.i. Wu, H. Yang, Q. Wu, Y. Yang, Z. He, Adsorption and competition mechanism of tetracycline and erythromycin on montmorillonite: experimental and theoretical investigation, J. Mol. Liq. 370 (2023), 121037.
[22] O.A. Olalekan, A.J. Campbell, A. Adewuyi, W.J. Lau, O.G. Adeyemi, Synthesis and application of ZnO-MgO-NiO@ Stearicamide mixed oxide for removal of ciprofloxacin and ampicillin from aqueous solution, Results Chem. 4 (2022), 100457.
[23] S.S. Mosavi, E.N. Zare, H. Behniafar, M. Tajbakhsh, Removal of Amoxicillin Antibiotic from Polluted Water by a Magnetic Bionanocomposite Based on Carboxymethyl Tragacanth Gum-Grafted-Polyaniline, Water 15 (2023) 202.
[24] Z. Huang, X. Fang, S. Wang, N. Zhou, S. Fan, Effects of KMnO4 pre-and post-treatments on biochar properties and its adsorption of tetracycline, J. Mol. Liq. 373 (2023), 121257.
[25] T.G.F. Souza, S.J. Olusegun, B.R.L. Galvão, J.L.F. Da Silva, N.D.S. Mohallem, V.S. T. Ciminelli, Mechanism of amoxicillin adsorption by ferrihydrites: experimental and computational approaches, J. Mol. Liq. 373 (2023) 121202.
[26] S.R. Ali, M.C. Arya, K. Abul, A.G. Al-Sehemi, K. Zenab, A. Sadaf, K. Rajesh, Adsorption potential of zirconium-ferrite nanoparticles for phenol, 2-chlorophenol and 2-nitrophenol: thermodynamic and kinetic studies, Desalin. Water Treat. 179 (2019) 183–196.
[27] N. Nasseh, B. Barikbin, L. Taghavi, M.A. Nasseri, Adsorption of metronidazole antibiotic using a new magnetic nanocomposite from simulated wastewater

(isotherm, kinetic and thermodynamic studies), Compos. B Eng. 159 (2019) 146–156.
[28] P. Caetano, N.M. Simões, P.S. Pinto, L.E. Fernandez-Outon, A.S. Albuquerque, W. A. Macedo, J.D. Ardisson, Application of nickel ferrite nanoparticles in adsorption of amoxicillin antibiotic, J. Braz. Chem. Soc. 31 (2020) 2452–2461.
[29] J. Ren, Z. Zhu, Y. Qiu, F. Yu, T. Zhou, J. Ma, J. Zhao, Enhanced adsorption performance of alginate/MXene/CoFe2O4 for antibiotic and heavy metal under rotating magnetic field, Chemosphere 284 (2021), 131284.
[30] A. Adewuyi, R.A. Oderinde, Tartaric acid-modified CuFe2O4: Potential application in the purification of butylated hydroxyanisole and butylated hydroxytoluene-contaminated water, J. Mater. Res. 37 (2022) 3033–3048.
[31] A. Adewuyi, C.A. Gervasi, M.V. Mirífico, Synthesis of strontium ferrite and its role in the removal of methyl orange, phenolphthalein and bromothymol blue from laboratory wastewater, Surf. Interfaces 27 (2021), 101567.
[32] E. Lima, E. De Biasi, M.V. Mansilla, M.E. Saleta, M. Granada, H.E. Troiani, F. Effenberger, L. Rossi, H. Rechenberg, R.D. Zysler, Heat generation in agglomerated ferrite nanoparticles in an alternating magnetic field, J. Phys. D Appl. Phys. 46 (2012), 045002.
[33] E. Burgaz, A. Erciyes, M. Andac, O. Andac, Synthesis and characterization of nano-sized metal organic framework-5 (MOF-5) by using consecutive combination of ultrasound and microwave irradiation methods, Inorg. Chim. Acta 485 (2019) 118–124.
[34] S.M. Mirsoleimani-azizi, P. Setoodeh, S. Zeinali, M.R. Rahimpour, Tetracycline antibiotic removal from aqueous solutions by MOF-5: Adsorption isotherm, kinetic and thermodynamic studies, J. Environ. Chem. Eng. 6 (2018) 6118–6130.
[35] A. Nasiri, S. Rajabi, A. Amiri, M. Fattahizade, O. Hasani, A. Lalehzari, M. Hashemi, Adsorption of tetracycline using CuCoFe2O4@ Chitosan as a new and green magnetic nanohybrid adsorbent from aqueous solutions: Isotherm, kinetic and thermodynamic study, Arab. J. Chem. 15 (2022), 104014.
[36] V.T. Lam, T.C.Q. Ngo, L.G. Bach, Facile fabrication of novel NiFe2O4@ carbon composites for enhanced adsorption of emergent antibiotics, Materials 14 (2021) 6710.
[37] M. Aghazadeh, A.N. Golikand, M. Ghaemi, Synthesis, characterization, and electrochemical properties of ultrafine β-Ni (OH) 2 nanoparticles, Int. J. Hydrogen Energy 36 (2011) 8674–8679.
[38] A. Adewuyi, A.I. Ogagbolo, W.J. Lau, R.A. Oderinde, Synthesis of spinel ferrite and its role in the removal of free fatty acids from deteriorated vegetable oil, Chin. J. Chem. Eng. 40 (2021) 78–87.
[39] S.A. Tirmizi, A. Badshah, H.M. Ammad, M. Jawad, S.M. Abbas, U.A. Rana, S.-U.-D. Khan, Synthesis of highly stable MOF-5@ MWCNTs nanocomposite with improved hydrophobic properties, Arab. J. Chem. 11 (2018) 26–33.
[40] G. Chen, J. Luo, M. Cai, L. Qin, Y. Wang, L. Gao, P. Huang, Y. Yu, Y. Ding, X. Dong, Investigation of metal-organic framework-5 (MOF-5) as an antitumor drug oridonin sustained release carrier, Molecules 24 (2019) 3369.
[41] L. Zhu, X. Jia, H. Bian, T. Huo, Z. Duan, Y. Xiang, D. Xia, Structure and adsorptive desulfurization performance of the composite material MOF-5@ AC, New J. Chem. 42 (2018) 3840–3850.
[42] C. Hammond, The Basics of Crystallography and Diffraction, Oxford Univ. Press, New York, 1997.
[43] A.T. Bell, The impact of nanoscience on heterogeneous catalysis, Science 299 (2003) 1688–1691.
[44] M. Shang, W. Wang, S. Sun, L. Zhou, L. Zhang, Bi2WO6 nanocrystals with high photocatalytic activities under visible light, J. Phys. Chem. C 112 (2008) 10407–10411.
[45] K. Nadeem, M. Shahid, M. Mumtaz, Competing crystallite size and zinc concentration in silica coated cobalt ferrite nanoparticles, Prog. Nat. Sci.: Mater. Int. 24 (2014) 199–204.
[46] H. Asadevi, P. Prasannakumaran Nair Chandrika Kumari, R. Padmavati Amma, S. A. Khadar, S. Charivumvasathu Sasi, R. Raghunandan, ZnO@ MOF-5 as a fluorescence "Turn-Off" sensor for ultrasensitive detection as well as probing of Copper (II) ions, ACS Omega 7 (15) (2022) 13031–13041.
[47] P. Sivakumar, R. Ramesh, A. Ramanand, S. Ponnusamy, C. Muthamizhchelvan, Synthesis, studies and growth mechanism of ferromagnetic NiFe2O4 nanosheet, Appl. Surf. Sci. 258 (17) (2012) 6648–6652.
[48] P. Sivakumar, R. Ramesh, A. Ramanand, S. Ponnusamy, C. Muthamizhchelvan, Synthesis and characterization of NiFe2O4 nanosheet via polymer assisted co-precipitation method, Mater. Lett. 65 (3) (2011) 483–485.
[49] K.K. Senapati, S. Roy, C. Borgohain, P. Phukan, Palladium nanoparticle supported on cobalt ferrite: An efficient magnetically separable catalyst for ligand free Suzuki coupling, J. Mol. Catal. A Chem. 352 (2012) 128–134.
[50] L. Tian, J. Zhang, H. Shi, N.a. Li, Q. Ping, Adsorption of malachite green by diatomite: equilibrium isotherms and kinetic studies, J. Dispers. Sci. Technol. 37 (7) (2016) 1059–1066.
[51] A. Terdputtakun, O.-A. Arqueropanyo, P. Sooksamiti, S. Janhom, W. Naksata, Adsorption isotherm models and error analysis for single and binary adsorption of Cd (II) and Zn (II) using leonardite as adsorbent, Environ. Earth Sci. 76 (2017) 1–11.
[52] J. Sirajudeen, J. Naveen, S.A. Manikandan, M.M. Mubashir, Removal of chromium (VI) from aqueous solution by using Citrus limetta peel as an adsorbent, Der Chemica Sinica 4 (2013) 133–143.
[53] T. Zhu, T. Van Voorhis, Understanding the dipole moment of liquid water from a self-attractive Hartree decomposition, J. Phys. Chem. Lett. 12 (1) (2021) 6–12.
[54] N.O. Obi-Egbedi, I.B. Obot, Xanthione: A new and effective corrosion inhibitor for mild steel in sulphuric acid solution, Arab. J. Chem. 6 (2) (2013) 211–223.
[55] D.I. Njoku, I. Ukaga, O.B. Ikenna, E.E. Oguzie, K.L. Oguzie, N. Ibisi, Natural products for materials protection: corrosion protection of aluminium in hydrochloric acid by Kola nitida extract, J. Mol. Liq. 219 (2016) 417–424.
[56] H. Wang, X. Wang, H. Wang, L. Wang, A. Liu, DFT study of new bipyrazole derivatives and their potential activity as corrosion inhibitors, J. Mol. Model. 13 (1) (2006) 147–153.
[57] A. Dwivedi, N. Misra, Quantum chemical study of Etodolac (Lodine), Der Pharma Chemica 2 (2010) 58–65.
[58] D. Balarak, F.K. Mostafapour, H. Azarpira, A. Joghataei, Mechanisms and equilibrium studies of sorption of metronidazole using graphene oxide, J. Pharmaceut. Res. Int. 19 (2017) 1–9.
[59] H. Abbas, A.S. Abbas, Adsorption of Flagyl on Prepared Ash from Rice Husk, Iraqi J. Chem. Pet. Eng. 22 (2021) 11–17.
[60] I. Kariim, A.S. Abdulkareem, O.K. Abubakre, Development and characterization of MWCNTs from activated carbon as adsorbent for metronidazole and levofloxacin sorption from pharmaceutical wastewater: kinetics, isotherms and thermodynamic studies, Sci. Afr. 7 (2020) e00242.
[61] A. Ahmadfazeli, Y. Poureshgh, Y. Rashtbari, H. Akbari, P. Pourali, A. Adibzadeh, Removal of metronidazole antibiotic from aqueous solution by ammonia-modified activated carbon: adsorption isotherm and kinetic study, J. Water, Sanitation Hygiene Develop. 11 (2021) 1083–1096.
[62] A. Amouei, D. Naghipour, K. Taghavi, M. Estaji, Removal of Metronidazole Antibiotic from Hospital Wastewater by Biosorbent Prepared from Plantain Wood, J. Babol Univ. Med. Sci. 22 (2020) 45–52.
[63] M. Malakootian, A. Nasiri, H. Mahdizadeh, Metronidazole adsorption on CoFe2O4/Activated Carbon@ Chitosan as a new magnetic biocomposite: modelling, analysis, and optimization by response surface methodology, Desalin. Water Treat. 164 (2019) 215–227.
[64] D. Parashar, A. Harafan, G. Achari, M. Kumar, Ciprofloxacin and Metronidazole Adsorption on Chitosan-Modified Graphene Oxide as Single-Compound and Binary Mixtures: Kinetics Isotherm, and Sorption Mechanism, J. Hazardous, Toxic, Radioactive Waste 27 (2023) 04022042.
[65] N. Aarab, A. Hsini, A. Essekri, M. Laabd, R. Lakhmiri, A. Albourine, Removal of an emerging pharmaceutical pollutant (metronidazole) using PPY-PANi copolymer: kinetics, equilibrium and DFT identification of adsorption mechanism, Groundw. Sustain. Dev. 11 (2020), 100416.
[66] Y.S. Açıkel, Investigation of adsorption of metronidazole on Chitosan-Halloysite nanocomposites and controlled release, Indian J. Chem. Technol. (IJCT) 27 (2020) 101–115.
[67] D. Balarak, F.K. Mostafapour, A. Joghataei, Experimental and kinetic studies on penicillin G adsorption by Lemna minor, Br. J. Pharm. Res. 9 (2016) 1–10.
[68] H. Nourmoradi, A. Daneshfar, S. Mazloomi, J. Bagheri, S. Barati, Removal of Penicillin G from aqueous solutions by a cationic surfactant modified montmorillonite, MethodsX 6 (2019) 1967–1973.
[69] S. Rahdar, A. Rahdar, M. Khodadadi, S. Ahmadi, Error analysis of adsorption isotherm models for penicillin G onto magnesium oxide nanoparticles, Appl. Water Sci. 9 (2019) 1–7.
[70] F. Masoudi, M. Kamranifar, A. Naghizadeh, The efficiency of Chitosan Extracted from Persian Gulf Shrimp Shell in Removal of Penicillin G Antibiotic from Aqueous Environment, Iran. J. Chem. Chem. Eng. 39 (2020) 235–244.
[71] S. Ahmadi, C. Adaobi Igwegbe, Kinetic Studies on penicillin G removal from aqueous environments by cupric oxide nanoparticles, Arch. Hygiene Sci. 10 (1) (2021) 86–96.
[72] M. Meksi, H. Kochkar, Penicillin G Adsorption Isotherms and Kinetic Studies Using TiO2 Nanotubes Free and Modified with β-Cyclodextrin, Chem. Lett. 44 (10) (2015) 1289–1291.
[73] H. Pouretedal, N. Sadegh, Effective removal of amoxicillin, cephalexin, tetracycline and penicillin G from aqueous solutions using activated carbon nanoparticles prepared from vine wood, Journal of Water, Process. Eng. 1 (2014) 64–73.